Laura Marx, BSc.

Biaxial Properties of Healthy Aortic Tissue Layers

MASTER'S THESIS

to achieve the university degree of

Diplom-Ingenieurin

Master's degree programme: Biomedical Engineering

submitted to

Graz University of Technology

Supervisor

Dipl.-Ing. Dr.techn., Gerhard Sommer

Institute of Biomechanics

M.Sc.RWTH, Justyna Anna Niestrawska

Graz, February 2016

AFFIDAVIT

I declare that I have authored this thesis independently, that I have not used other than the declared sources/resources, and that I have explicitly indicated all material which has been quoted either literally or by content from the sources used. The text document uploaded to TUGRAZonline is identical to the present master‘s thesis dissertation.

Date

Signature

Contents

List of Tables

List of Figures

Abstract

A leading cause for significant cardiovascular morbidity and mortality worldwide are diseases of the aorta. The occurance of aortic disease shows an upward trend in relation to the advancing age of the population. It is known that mechanics play a significant role in arterial diseases as mechanical properties tend to change with pathological symptoms. Even so advances during the past two decades have increased our knowledge of mechanics and biology of the human abdominal aorta, yet there remains a pressing need for considerable new data. Thus, the focus of this thesis lies on the execution of biaxial tensile tests to examine the layer specific mechanical properties of human abdominal aortas to better understand the underlying biomechanics and mechanobiology of the tissue. This may be useful for clinical applications such as the improvement of diagnosis and treatment of vascular diseases along with injuries.

All the human arterial tissue samples used for the experiments were received from the Department of Pathology, University Hospital Graz, Austria. Specimen of the individual layers (intima, media and adventitia) and the composite of each sample were first prepared in a square shape (20x20 mm) and subsequently in a cruciform manner, mounted into the testing device and tested biaxially at different stretch levels and ratios. Data received from the performed measurements was evaluated through computation of the Cauchy stresses, which where additionally plotted as a function of stretch. For a descriptive statistical analysis the median and interquartile range (IQR) were calulated and visualised as box-and-whisker plots. The mechanical behavior of the individual samples as well as the layers and the composite were compared under consideration of potential influencing factors such as age, gender and specimen geometry.

The distinct influence of age on the mechanical behavior of the tissue, in terms of stiffening, could only be shown for the media. A change in mechanical behavior due to gender differences of the donors could not be observed. The geometry of the samples showed an major impact on the mechanical behavior, namely observed higher Cauchy stresses for the cruciform specimen. All layers showed an anisotropic, linear elastic behavior in lower stress regions followed by non-linear stiffening at higher stretch levels.

Zusammenfassung

Erkrankungen der Aorta sind eine maßgebliche Ursache für eine weltweite Morbidität und Mortalität, deren Auftreten mit dem fortschreitenden Alter der Bevölkerung steigt. Dabei spielt die Mechanik des Gewebes eine entscheidende Rolle, da sich die mechanischen Eigenschaften mit pathologischen Symptomen verändern. Obgleich des Wissensfortschritts im Bereich der Mechanik und Biologie der humanen abdominalen Aorta in den vergangenen zwei Jahrzehnten, verbleibt die Notwendigkeit für die Generierung neuer Daten. Demzufolge liegt der Fokus dieser Masterarbeit auf der Ausführung biaxialer Zugversuche um die schicht-spezifischen mechanischen Eigenschaften humaner abdominaler Aorten zu untersuchen und die zugrundeliegende Biomechanik und Mechanobiologie dieses Gewebes besser zu verstehen. Dies könnte sich für klinische Anwendungen, wie etwa Verbesserungen im Bereich der Diagnostik und Behandlung von vaskulären Erkrankungen nebst Verletzungen, als nützlich erweisen.

Die gesamten humanen Gewebeproben der Aorten, welche für die Experimente verwendet wurden, stammten vom Institut für Pathologie, LKH Graz, Österreich. Einzelproben der Arterienschichten und der Verbundstruktur wurden in quadratischer Form (20x20 mm) und in später Folge auch als Kreuzprobe biaxial unter verschiedenen Dehnungsbedingungen (Stretchlevels) und Verhältnissen (Ratios) getestet. Die durch die ausgeführten Messungen generierten Daten wurden durch Berechnung der Cauchy-Spannungen und der graphischen Darstellung als Spannungs-Dehnungs-Diagramme analysiert. Zur deskriptiven statistischen Auswertung jener Daten wurde der Median und Interquartil-Bereich der maximalen Cauchy-Spannungen kalkuliert und in Form von Kastengrafiken dargestellt.

Der deutlich sichtbare Einfluss des Alters auf das mechanische Verhalten dieses Gewebes, im Sinne einer Versteifung, konnte nur für die Media, die mittlere Schicht der Arterienwand, gezeigt werden. Eine Veränderung des mechanischen Verhaltens aufgrund des Geschlechts der Patienten konnte nicht festgestellt werden. Die Geometrie der Proben hingegen schien eine erhebliche Auswirkung auf die mechanische Antwort des Gewebes zu haben. Kreuzförmige Proben zeigten deutlich höhere maximale Cauchy-Spannungen. Alle Schichten als auch die Verbundstruktur zeigten ein anisotropes, linear elastisches Verhalten in niedrigen Spannungsbereichen, jedoch eine nicht-lineare Versteifung in höheren Spannungsregionen.

Acknowledgment

My profound gratitude goes to my superviser Dipl.-Ing. Dr.techn. Gerhard Sommer and my co-superviser M.Sc. Justyna Anna Niestrawska who helped me in so many ways with the successful completion of this master thesis. I could count on their support, guidance, expertise and knowledge throughout the laboratory work, the data evaluation process and the whole period of writing this thesis. Special thanks go to my co-superviser for her very valuable comments and unfailing patience.

Further, I want to express my gratitude to the head of the Insitute of Biomechanics, Technical University Graz, Austria, Univ.-Prof. Dipl.-Ing. Dr.techn. Gerhard A. Holzapfel, who gave me the opportunity to carry out the experimental work by providing the laboratory facilities. Thank you for the opportunity to be a part of this research project!

Finally, I am more than grateful to my parents supplying me with the opportunity to study in the first place, for always being supportive and understanding. Likewise I want to thank my sister and friends for their continuous encouragement throughout my years of study as well as during the process of writing this master thesis.

1 Introduction

The field of biomechanics enables us to unterstand many biophysical phenomena on the molecular, cellular, tissue, organ, and organism levels. Better knowledge of the biomechanical properties and behavior of materials may be used for clinical applications in terms of better prevention of injury, improved diagnostics, treatment of diseases as well as surgical planning and intervention. Experimental biomechanics, which is a challenging and important discipline, provides information through experiments, that is essential for formulating constitutive relations and for proposing and evaluating broader theoretical concepts. The information can also be used to solve many boundary value and initial value problems, which are of great importance [1]. Therefore, the focus of this research lies on the execution of biaxial tensile tests to examine the layer specific mechanical properties of human abdominal arteries in order to investigate the underlying biophysical phenomena on the tissue level. The identification of the layer specific biomechanical properties may be useful for clinical applications.

It is known that mechanics play a significant role in arterial diseases as the mechanical properties tend to change with pathological symptoms. Advances during the past two decades have increased our knowledge of mechanics and biology of the human abdominal aorta, yet there remains a pressing need for considerable new data [2]. Thus, the main aim of this thesis is to better understand the underlying biomechanics and mechanobiology of abdominal aortic tissue in order to improve diagnosis and treatment of vascular diseases along with injuries.

A leading cause for significant cardiovascular morbidity and mortality worldwide are diseases of the aorta. The occurance of aortic disease shows an upward trend in relation to the advancing age of the population. As the aorta is the biggest artery in the body and the main channel for supply the importance for this vessel to function is evident. There are many diseases and conditions affecting the aorta causing a life threatening risk. Atherosclerosis, hypertension, genetic conditions, connective tissue disorders as well as injury can have a fatal effect on the human health. In case of disease the aorta may dilate, leading to aneurysms, dissect or even rupture causing sudden death. Risk factors such as a family history of vascular diseases, high blood pressure, smoking, diabetes, being overweight, high cholesterol levels, an unhealthy diet, lack of exercise, stress and age can be set in a direct context to an accelerated progression of vascular diseases. In general there is a higher risk for men to develop some sort of vascular disease. [3], [4], [5]

Considering the great necessity to comprehend how those diseases occur it is essential to do more research in the field of the vascular mechanics to find out more about the structure and the behavior of this certain tissue. Arterial tissue or soft biological tissue in gerneral is incompressible meaning that there is no volume change under physiological deformation [6]. This implies that under the incompressibility assumption the mechanical properties of a three-dimensional specimen can be determined completely by two-dimensional tests [7]. Hence, an effective technique to characterize the layer specific material properties of abdominal arteries are planar biaxial tension tests [8].

Studies about the mechanical behavior of arteries have been focus of research over the last 100 years. Anyhow, the first to consider the heterogeneity of the arterial tissue, in terms of individual layers, were [9]. Since then most studies were based on animal tissue, which differs from human arterial tissue. In human arterial tissue the intima, most inner layer, tends to grow and is subject to change, in terms of stiffening, with advancing age. Anyhow, the mechanical testing of this fragile layer remains a challenge. The lastest data about the mechanical properties of different arterial tissues comes from the group of Holzapfel. [10]

'There are relatively few data on the mechanical properties of arterial tissues, especially for the separate layers of a vessel wall, and the material-testing protocols have varied between the measurements that have been published.' [11]

As part of a research project of the Institute of Biomechancis, Technical University Graz, Austria, in cooperation with the Institute of Pathology, LKH Graz, Austria, the aim of this thesis is the performance of layer specific biaxial tensile test in a planar manner in order to collect considerable new data about the heterogeneous mechanical behavior of the arterial wall. Different loading protocols are to be used to generate data of the direction-dependent material response. The received mechanical data in combination with the present structural knowledge of the individual layers of the arterial wall should give more insight on their specific functions.

To clearly understand the tissue's mechanical properties and reaction to load it is essential to have a certain knowledge about the structure and composition of human arteries. Therefore the fundamentals of the human arteries are summed up in chapter 2 along with a backround on mechanical testing of soft tissues and their general mechanical properties. An overview of the methods used for the experiments and data evaluation is presented in chapter 3. The results obtained for all samples tested and the individual layers can be found in chapter 4 and are discussed in chapter 5, where concluding remarks are made and the future outlook on this study is shown.

2 Background

Human arteries can be divided into three major groups according to their size and the characteristics of the middle layer, the media: Elastic, muscular and small arteries, and arterioles. The group of elastic arteries includes the pulmonary arteries, which transport blood away from the heart to the systemic as well as the pulmonary circulation and the aorta with the abdominal region being focus of this study. Elastic arteries are the largest arteries (greater than 10 mm in diameter) in the human body, which contain multiple sheets of elastic lamellae in their walls. Anyhow, a clear distinction between the already mentioned elastic arteries and the muscular type is hardly possible because of their intermediate features. Small arteries differ from arterioles solely by the number of smooth muscle layers. [12]

In the following chapter the underlying function as well as the structure of elastic arteries is outlined (see section 2.1 and 2.2) along with the components of the arterial wall (see section 2.3), the mechancis of soft biological tissue (see section 2.5) and the theory of mechanical testing (see section 2.5.1).

2.1 Function of Elastic Arteries

Elastic arteries fulfill the Windkessel function, changing the intermittent blood output of the heart into a continuos flow. This demands reversible elastic wall properties so that the arteries are able to distend during systole, the contracting phase of the cardiac cycle, where blood is pumped from the ventricles into the elastic arteries. The limit of this distension is given by the network of collagen fibers situated in the tunica media and tunica adventitia. [12]

To maintain the arterial blood pressure and the flow within the vessels during diastole, the relaxation phase of the cardiac cycle, the recoil of the distended arteries is essential. Considering rigid wall properties these distension and recoil mechanisms would become impossible leading to a higher blood pressure and thickening of walls. More distal from the heart the elastic properties decrease with the percentage of elastic fibers whereas the smooth muscle in the tunica media increases leading to muscular arteries. [12], [13]

2.2 Structure of Elastic Arteries

The arterial wall structure is composed of three layers, namely the tunica intima, the tunica media and the tunica adventitia (see Fig. 2.1). [12]

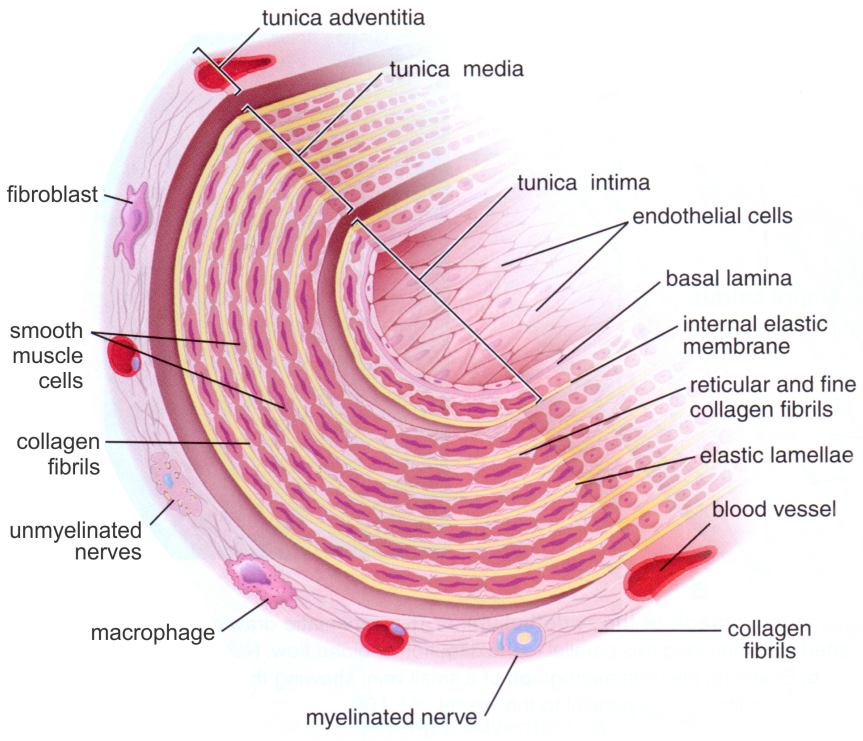

Figure 2.1: Structure of an elastic artery. The schematic drawing shows the three individual tissue layers including their components. Taken from [12].

The tunica intima of elastic arteries consists of the endothelium, the subendothelial layer and the internal elastic membrane. The luminal surface of the endothelium is covered with endothelial cells (endothelial lining) connected to the basal lamina. The endothelial cells are flattened, elongated and orientated with their long axis in a parallel manner to the direction of blood flow forming an interconnection via tight or gap junctions as shown in Fig. 2.2. [12]

In case of damage of this endothelial lining the blood is exposed to the collagenous fibers beneath causing blood clot formation. For a long time the endothelium seemed to be a simple physical boundary between the blood in the lumen and subendothelial tissue. Recent studies, however, have shown that it is physiologically critical to such activities as helping to regulate capillary exchange and altering blood flow. The endothelium releases local chemicals called endothelins that can constrict the smooth muscle within the walls of

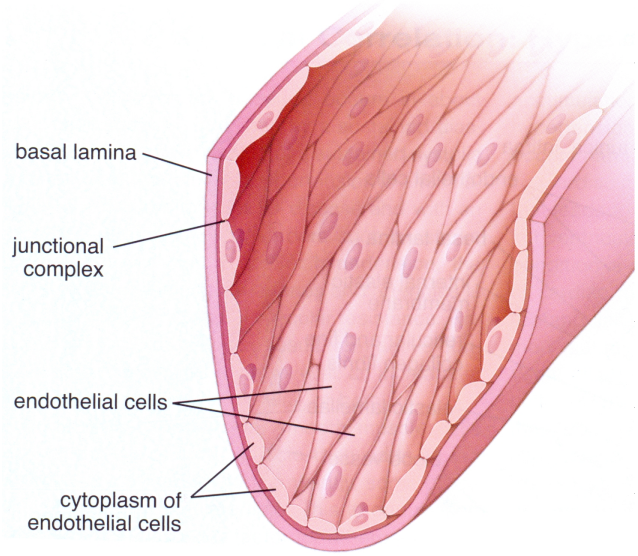

Figure 2.2: Structure of the endothelium. The schematic drawing shows the endothelial lining and the basal lamina. Taken from [12].

the vessel to increase blood pressure. Uncompensated overproduction of endothelins may contribute to hypertension (high blood pressure) and cardiovascular disease. [13], [12]

The subendothelial layer adjacent to the endothelium is basically a connective tissue layer including both collagen and elastic fibers. The thickness varies with topography (e.g. almost non-existent in healthy muscular arteries), disease and age [7]. The internal elastic membrane cannot be easily distinguished as there are numerous elastic layers present in the wall of this certain type of artery [12]. As the intima is very thin at a healthy state it is not contributing significantly to the solid mechanical properties of the arterial wall. With advancing age the intima tends to thicken and stiffen possibly making its mechanical contribution more important. [7]

The tunica media is the thickest layer and consists of concentric elastic lamellae (elastin) inbetween numerous layers of smooth muscle cells (see Fig. 2.1). Diffusion of substances within the arterial wall is facilitated by the fenestrations of the lamella. The thickness as well as the number of lamellae increase with rising blood pressure and advancing age. The same occurs in case of hypertension [12]. With decreasing vessel size, vessels more distal from the heart, a decrease in the number of lamellae can be observed [7]. Synthesis of collagen, elastin and other components of the extracellular matrix is done by the smooth muscle cells, spindle-shape cells with an elongated nucleus. In response to certain growth factors, synthesized by endothelial cells, it can occur that the smooth muscle cells proliferate or even migrate to the tunica intima playing an aiding or rather contributing role in

normal vascular wall repair and in pathological processes. As the cells within the smooth muscle layers are able to contract a certain prestress within the elastic lamella system is noticeable. The above described structure of lamellae and smooth muscle cell layers receives its stability from collagen fibers and is embedded into a proteoglycan rich ground substance [12]. Mechanically, the media can be seen as the most significant layer considering its high strength, resilience and ability to resist loads in the axial as well as the circumferential direction. [7]

The tunica adventitia, a connective tissue layer, anchors the artery to surroundings. It contains an unorganized elastic fibre network, composed of collagen and elastic fibers, and fibroblasts as well as macrophages. This layer of the vascular wall is rich on vasa vasorum, tiny veins and arteries sometimes also entering the outer part of the tunica media, and nerves. [12]

The unloaded adventitia at low pressure does not reach the stiffness of the media by far. As pressure increases the wavy collagen fibres, arranged in helices, are fully straightened leading to an significant increase of stiffness [7]. Thus, mechanically the adventitia can be viewed as a protective sheath preventing over-distension of the arterial wall in order to avoid damage of the smooth muscle cells in the media [14]. Further the adventitia is thought to play major biological roles [15].

2.3 Components of the Arterial Wall

The arterial wall is composed of cellular and non-cellular components. Scleroproteins, namely collagen and elastin, smooth muscle cells and the ground substance contribute significantly to the overall mechanical response of arterial tissue [1].

Collagen is the main load-bearing element in all soft tissues and accounts for over 30% of the overall weight of proteins in the human body. 28 different types of collagen exist, where Types I, III-VI and VIII make up the majority of collagen fibres present in the cardiovascular system. Almost all connective tissues including arteries contain large structural bundles of collagen assembled by Type I and III collagen. Smooth muscle cells can be set in context with Type V and VI collagen whereas Type VIII collagen corresponds to endothelial cells. Each collagen molecule (tropocollagen), independent of its Type, is composed of three polypeptid strands, left-handed helices, arranged to form a right-handed triple-helix. The stabilization of this structures, called collagen fibrils, is given by intermolecular cross-links, namely hydrogen bonds, significantly contributing to the strength of the tissue (for a more detailed description of the organisation of collagen molecules see Fig. 2.3). Bundles of collagen fibrils further assemble to form collagen fibres, which possess a very high tensile strength altering with age and pathology. In blood vessels collagen fibres are organised in a concentrical fashion. In order for collagen to fulfill its physiologi-

cal function it is essential that synthesis and degradation of collagen is balanced. Different to elastin, whose generation occures during development and its degradation in relation to aging is expressed in stiffening of the arteries, collagen has a half-life of 15 to 90 days. [16], [17]

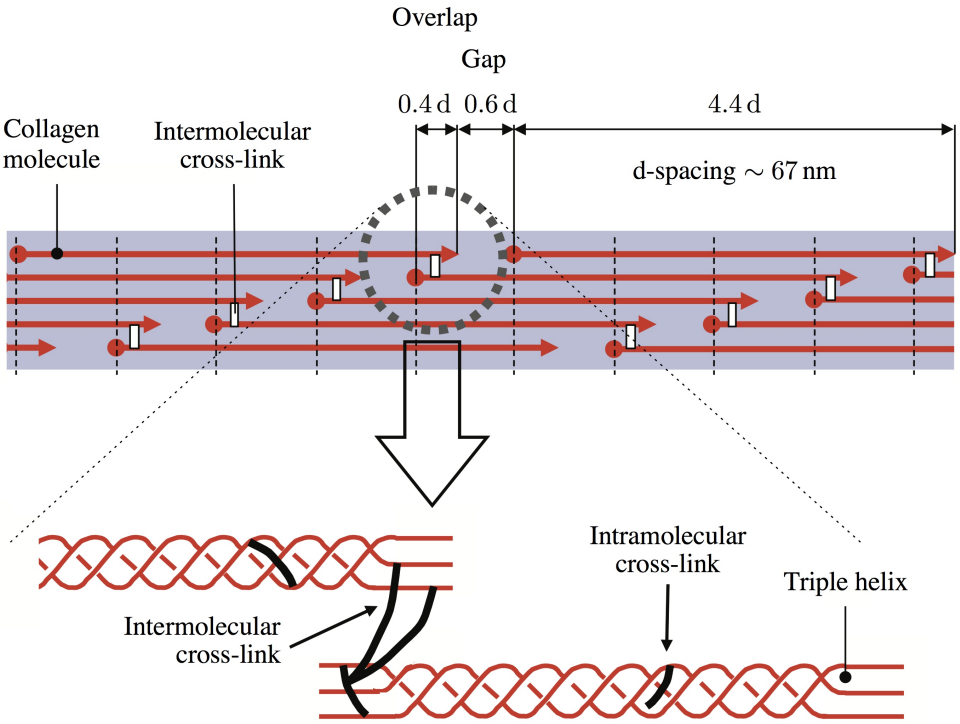

Figure 2.3: Detailed hierachical organisation of collagen molecules forming collagen fibrils. Taken from [16].

Elastin is a fibreprotein consisting of polypeptid subunits basically showing an linear elastic behavior when subjected to load. The mechanical response of elastin can be compared with the response of a rubber band. The highly cross-linked 3D network of the long flexible elastin molecules does not follow a certain hierachical organisation (see Fig. 2.4 (B)), which explains its isotropic behavior under load. Elastin is able to withstand extremely large strains without fracturing while only low stresses are needed to cause rupture of the collagen network. The ratio of elastin to collagen in the aortic wall strongly depends on its location in the human body. The content of elastin decreases away from the heart while the content of collagen is increasing (similar with aging). Elastin in arteries is synthesized by smooth muscle cells, fibroblast and propably endothelial cells. While elastin is thermally stable, the hydrogen bonds in collagen fibrils break at a certain temperature causing substantial structural changes. [16], [1]

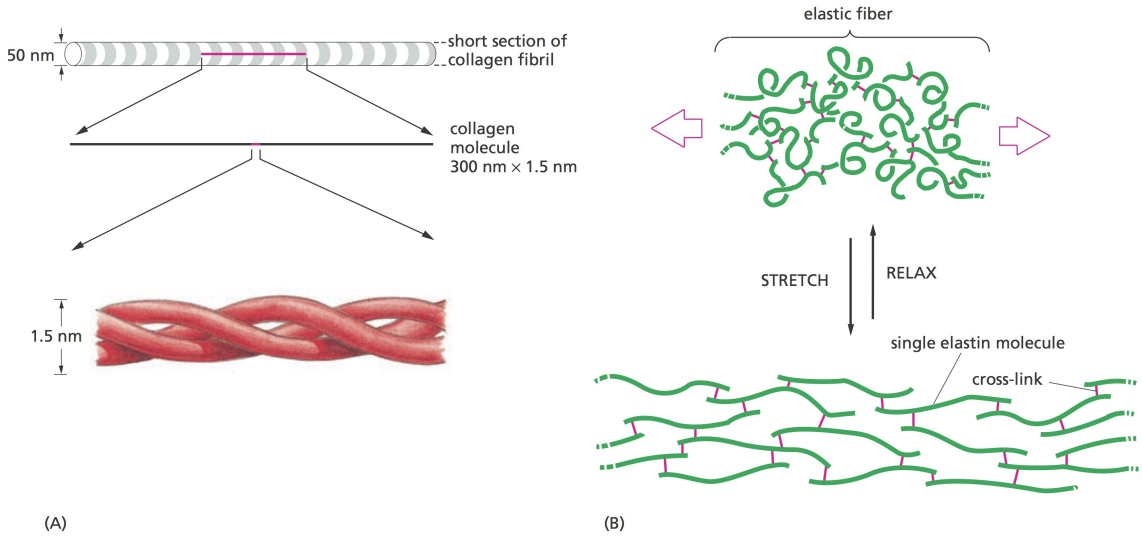

Figure 2.4: Comparison of organised structure of collagen (A) with elastin (B) following no hierachical organisation. Taken from [17].

Figure 2.5 shows the individual mechanical response of elastin and collagen through selective digestion as well as the overall response of a human external iliac artery. Collagen remains quite stiff showing highly non-linear characteristics behaving somewhat like a 'security scaffold'(elastin-digested curve). In turn elastin exhibits a linear elastic behavior (collagen-digested curve). The control curve corresponding to the overall response shows an almost linear behavior at low tension regions suggesting that elastin is the load bearing element. At higher loading domains collagen kicks in and non-linear stiffening of the artery becomes visible. [16]

The mechanical behavior of the spindle-shaped smooth muscle cells, 100 µm long and 5 µm in diameter, is influenced by its contraction state changing its geometrical configuration. Smooth muscle cells show a rather distinct nonlinear behavior and act highly viscoelastic. [1]

The gel like ground substance, composed of glycosaminoglycans, proteoglycans and water, serves as molecular filter and hence plays an important role in fluid flows. Nevertheless, its mechanical behavior does not show a meaningful contribution to the overall response of blood vessels. [1], [16]

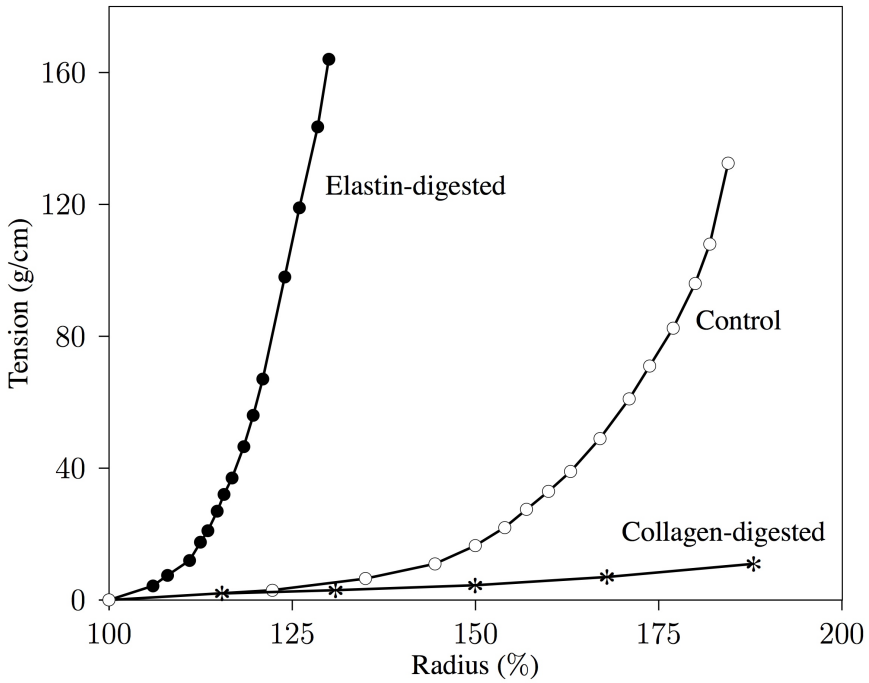

Figure 2.5: Tension-radius responses of human iliac arteries. The control response represents the untreated artery, the elastin-digested response the property of collagen and the collagen-digested response the property of the remaining elastin. Taken from [18] and modified by [16].

2.4 Abdominal Aorta

The aorta is the largest artery in the body where the most periphere part or often called final section, the abdominal aorta (or aorta abdominalis), is of focus in this thesis. The abdominal aorta arises from the thoracic artery commencing at the diaphragm and ends in a bifurcation forming the common iliac arteries (see Fig. 2.6) supplying the abdominal, pelvic organs and the legs with blood of high oxygen content. [9], [19]

2.5 Mechanics of Soft Biological Tissue

The term ‘Biomechancis’is composed of the words ‘Biology’and ‘Mechanics’which implies the definition according to [21] that Biomechanics is the development, extension and application of mechanics to answer questions of importance in biology and medicine.

In general soft tissues can be defined as anisotropic, meaning that the tissue has a preferred fibre direction, is incompressible, homogenous in a macroscopic sense but non homogenous in a microscopic sense and highly deformable. Soft tissues exhibit a viscoelastic behavior and a material response which is non linear stiffening. Furthermore material properties of soft tissue depend on the origin of tissue, the underlying function but also on the composition, namely the concentration and structural arrangement of its components [1]. The aorta, for example, with a high concentration of elastin compared to collagen provides this vessel with a high ultimate tensile strain in contrast to a rather low ultimate tensile strength. Besides, species, age and (vascular) risk factors have a considerable effect on the material properties of soft tissue. [8]

2.5.1 Theory of Mechanical Testing

Over the years various types of mechanical tests (for instance simple tension tests, equibiaxial tension tests, pure shear test, biaxial tension tests, torsion tests, extension and inflations tests) have been established to study the mechanical response and further characterize the properties of materials. For isotropic materials biaxial test are convenient making a complete characterization of the material properties possible. Anyhow, this is not sufficient for anisotropic material as some a priori assumptions have to be made in order to form more specialized constitutive laws and thus characterize the material properties fully. Mechanical tests can further be divided in two groups, quasi-static or dynamic, based on the strain rates. Depending on the way in which load is applied on the specimen tests can be classified as cyclical or discontinuous. [7], [8]

Considering that the mechanical behavior of arteries depends on temperature, osmotic pressure, pH, partial pressure of carbon dioxide and oxygen, ionic concentration and monosaccharide concentration the testing environment should be as similar as possible to the physiological conditions in vivo [7].

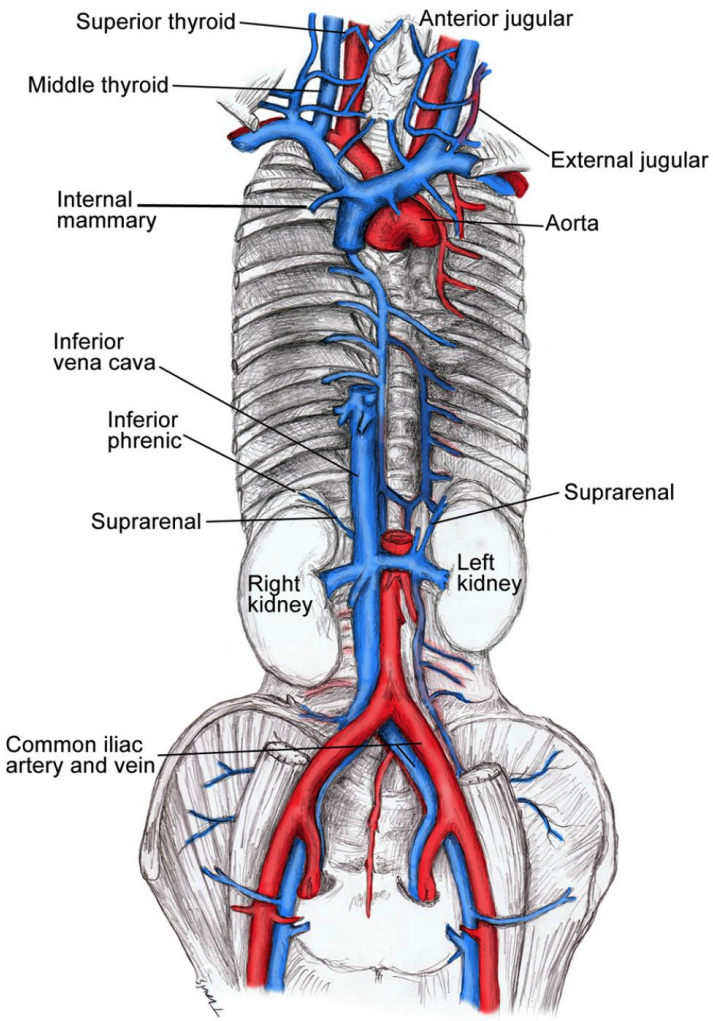

Figure 2.6: Anatomy of the aorta. The schematic drawing shows the individual branches of the abdominal aorta. Taken from [20].

3 Material and Methods

In order to achieve accurate and qualitative results the origin of the samples, appropriate transport, suitable storage, elaborate preparation of specimen and an accurate experimental setup is fundamental. To analayse and conclude thoroughly precise measurements are needed. Anyhow, several conditions may influence the measurements and their consideration is therefore outlined in this chapter.

3.1 Material

Througout this study human arterial tissue, precisely pieces of the abdominal aorta, from the Institute of Pathology, University Clinic Graz, Austria, was used. Samples were harvested from seven male patients and four female patients (for more details see table 3.1). As another research project at the Institute of Biomechanics, University of Technology Graz, Austria, examines the mechanical behavoir of the aortic tissue at a diseased state, namely AAAs, abdominal aortic aneurysms, the abdominal region of the aorta was chosen in order to make a comparison with healthy tissue of the same region possible. Considering the goal to study the behavior of healthy aortic tissue layers it was made sure that the patients did not have a history of vascular disease or disorders.

3.1.1 Transport and Storage

After the autopsy the samples were stored in PBS (phosphate-buffered-saline) solution and kept at 4°C until frozen at -20°C or processed. It had to be borne in mind that the cooling chain of the sample should not be interrupted at anytime as the arterial tissue is sensitive to temperature change. Approximately 12 hours before preparation the aortic tissue was thawed in the fridge at 4°C. Potential effects of storage on the mechanical behavior of the samples are discussed in 3.2.5.

Table 3.1: Overview of tested samples including sample ID, information about the patient (gender and age (G/A)), individual layers tested, their thickness (given in mm) and the specimen's size (given in mm) and geometry. Note that I stands for intima, M for media, A for adventitia, C for composite and cross for a cruciform specimen geometry (5x5 mm in the central region).

Sample ID	G/A		Layers tested				Thickness				Sample Size
	m	f	I	M	A	C	I	M	A	C	
A01	84			x	x	x		1.10	0.54	1.78	20x20
A02	45			x	x	x	0.21	0.84	0.70	1.90	20x20
A03	82			x	x	x		0.94	0.67	1.84	20x20
A04	67			x	x	x		1.08	1.15	3.22	20x20
A05		72		x	x	x		0.93	0.83	1.85	20x20
A06		61		x	x	x	0.43	0.57	0.59	1.83	20x20
A07	67			x	x	x		1.54	0.94	2.47	20x20
A08	49		x	x	x	x	0.35	1.17	0.49	1.85	20x20(A,C), cross(I,M)
A09		61		x	x	x	0.21	1.14	0.68	1.91	20x20
A10	56		x	x	x	x	0.29	0.82	0.53	1.72	cross
A11		63	x	x	x	x	0.38	1.26	1.58	2.86	cross

3.1.2 Specimen Design and Attachment Details

The biaxial tensile device is used to exert loads in two directions onto the tissue similar to those present in the human body to enable further investigation of these loads. The goal is to transfer test forces from the testing device onto the tissue as homogeneous as possible. According to [22] the specimen geometry and attachment details have a significant effect on the uniformity of the strain fields and in order to extract meaningful stress-strain data it is essential that the strain fields are relatively constant (ratio of principles strains $E_{11}/E_{22} < 1.10$). Therefore, [22] presented specific guidelines for specimen design and attachment suggesting a square shaped geometry having five attachment points per side placed 0.6 to 1.0 times the attachement point spacing away from the edge of each side. Attachment occured by means of sutures and commercial fisher hooks. Fig. 3.1 shows a simulation of how the strain field changes with the number of attachment points along each side.

Trying to follow these guidelines, which become even more crucial as the specimen size decreases, brought up a few difficulties. As the samples partly showed some sections of calification or bifurcations within the tissue, the area of the sample suitable for specimen preparation was restricted. Therefore, the initial sample size was chosen to be 20x20 mm, requiring an even more precise attachment point location (with an attachment point spacing of 3.0 mm and a distance from attachment points to the edge of 2.5 mm) achieved by usage

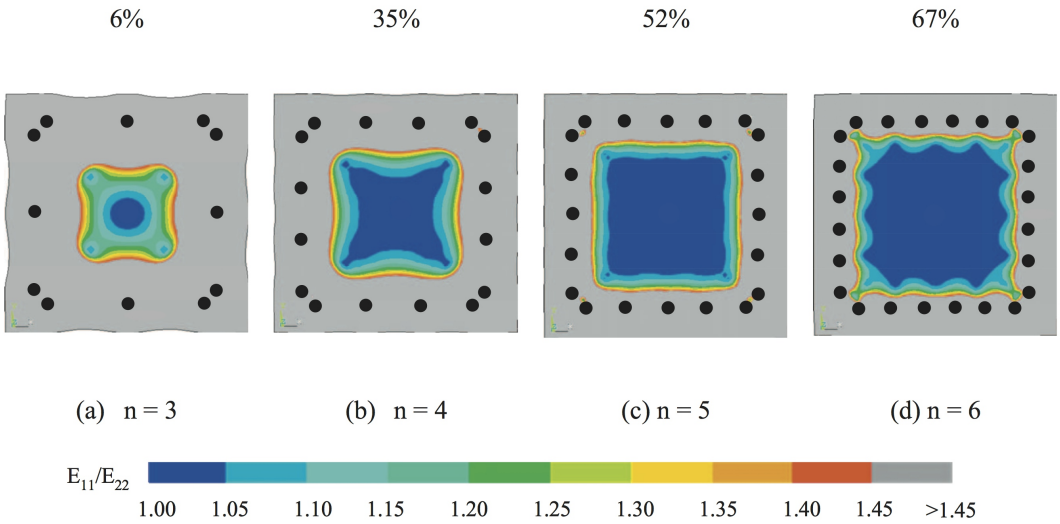

Figure 3.1: Changing the number of attachment points n along each side significantly changes the strain field inside the region they define, as indicated by the color contour plots of the principal strain ratio E_{11}/E_{22}. Taken from [22].

of a template made out plastic foil with mm scale (see Fig 3.2(a)). To test the more fragile layers, namley the intima and the adventitia, in this manner, turned out to be impossible as the tissue ruptured either during preparation, attachment or mounting.

In the course of Sherifova's study [23] showing the first steps towards modeling the propagation of aortic dissection, an optimal specimen geometry for biaxial tensile testing, namely a cruciform geometry with a reduced cross-section in the biaxially loaded zone, was designed, by modeling six geometries (A to F) under different boundary conditions using finite element analysis (see Fig 3.3). Simulations of boundary conditions occured equi-force controlled, equi-displacement controlled and displacement controlled with varying ratios in two directions. Goal was to achieve homogeneous stress distribution in the central area while minimizing the stress concentration in the arms. Geometries differ in thickness, radius between the arms and presence as well as style of symmetric cut in order to achieve stress flow towards the center. The orignal geometry A (see Fig 3.2 (b)) was modelled having a thickness of 1.2 mm. Geometry B (40% of original thickness), C (30% of original thickness), D (20% of original thickness) and F show a symmetric cut from the bottom and the top. Geometry F also shows a larger radius while geometry E (20% of original thickness) is only cut from one side. Best results were obtained for geometries with decreased thickness, symmetric cut and smaller radius between the arms (Geometry D). [23]

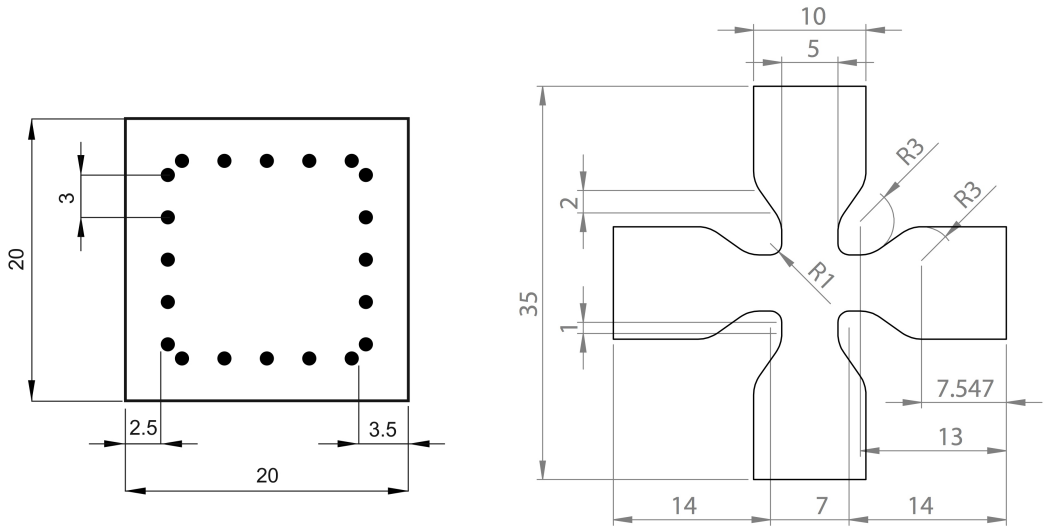

(a) Square shaped template with circles indicating the attachment points.

(b) Cruciform specimen.

Figure 3.2: Schematic drawings of different specimen geometries with dimensions given in mm. Figure (b) taken from [23].

Based on Sherifova's findings, the cruciform shape for the specimen was introduced (see Fig. 3.2 (b)) requiring the usage of a customized stamping device produced by Q-tec Gmbh, Zeilarn, Germany in combination with a fine press from TOX PRESSOTECHNIK GmbH & Co.KG, Weingarten, Germany. The attachment occured as described in section 3.1.3.

To prove that the stress-strain data is meaningful despite the specimen design and attachment differing from the guidelines of [22] for the square shaped specimen and the cruciform specimen the homogeinity of the strain field within the central region of the specimen was calculated according to [24] using a MATLAB Code [25]. The mathematical background for the quantification of the strain field is outlined in section 3.2.4 and the results are shown in chapter 4.

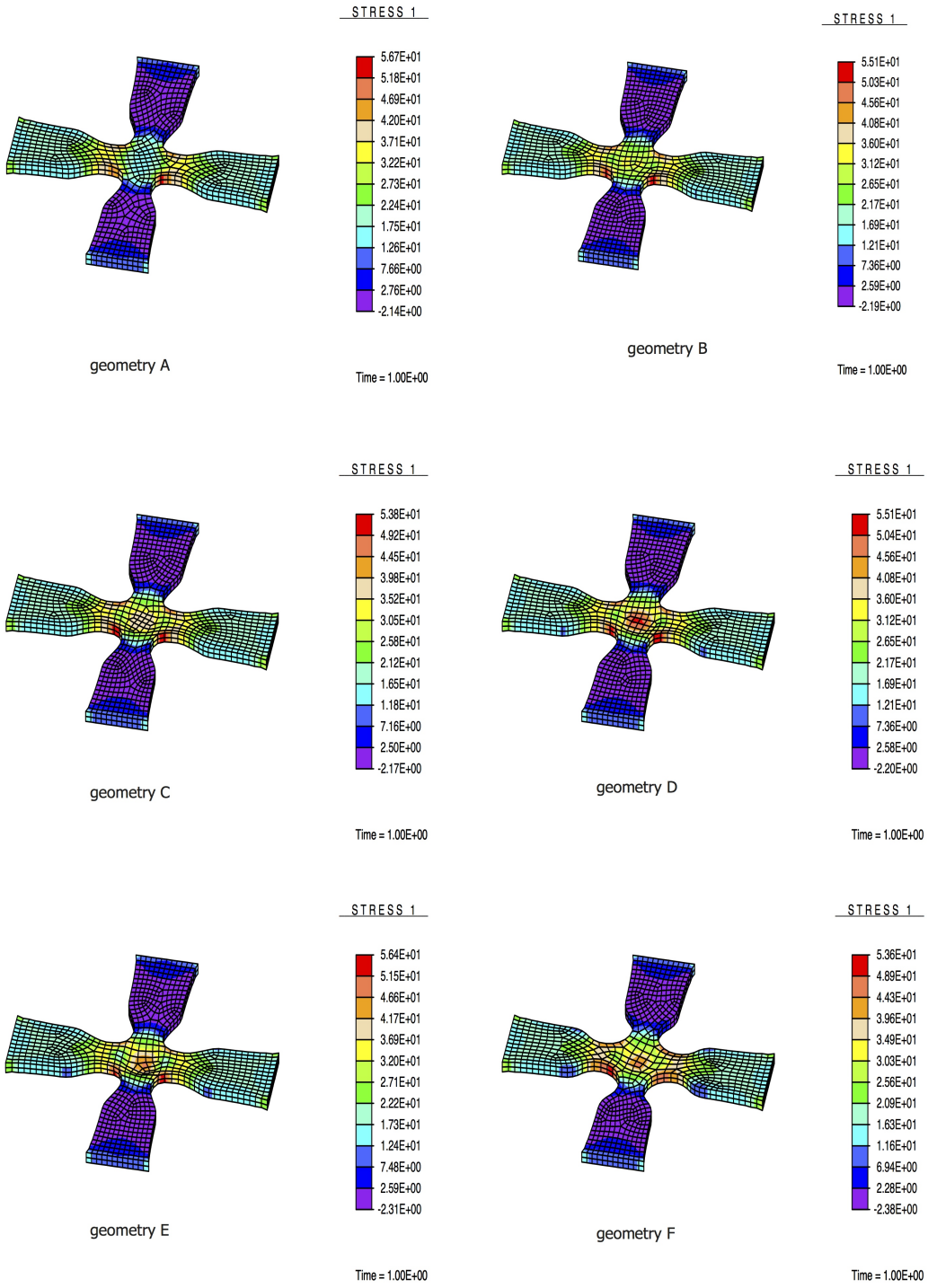

Figure 3.3: Result of simulation for cruciform-shaped specimen for all six geometries. Distribution of the stress in circumferential direction is presented (1:1 displacement ratio, maximum stretch of 20%). Taken from [23].

3.1.3 Specimen Preparation

During preparation the arterial tissue was kept moist by frequently sprinkling PBS solution on the specimen to prevent the tissue from drying. Goal was to prepare a specimen of the individual layers as well as a composite out of each sample. At first, all adipose tissue surrounding the abdominal aorta was removed using a scalpel and forceps taking care not to harm the adventitia, the outer most layer of the artery, as well as the adipose tissue itself as it was needed for a different research project. The artery then was cut open following its axis in order to receive a planar specimen. As mentioned in section 3.1.2 two different specimen geometries were used following a different process of preparation.

In case of the 20x20 mm square shaped specimen a pattern the same size (made out of a plastic foil with milimeter scale) was put on the specimen so that two sides of the square were oriented in the axial direction leaving the other two sides standing orthogonal to it. A dissection blade was used to cut the specimen into its final shape making sure to mark the axial direction by either drimming the edges or usage of the surgical pen. In this manner two 20x20 mm specimen were prepared, one being the composite and the other one for further preparation into the individual layers of the artery by pealing off each layer slowly using forceps (see Fig. 3.4 (a)). The pattern was used again to mark the position of the fisher hooks, five on each side connected through suture for mounting the specimen into the testing device (see section 3.1.2 for further information on the attachment details). Afterwards the hooks could be inserted into the tissue using forceps to hold up the tissue. This had to be done carefully in order to not harm the specimen. For particle tracking a thin layer of tissue marker paint was applied using an airbrush.

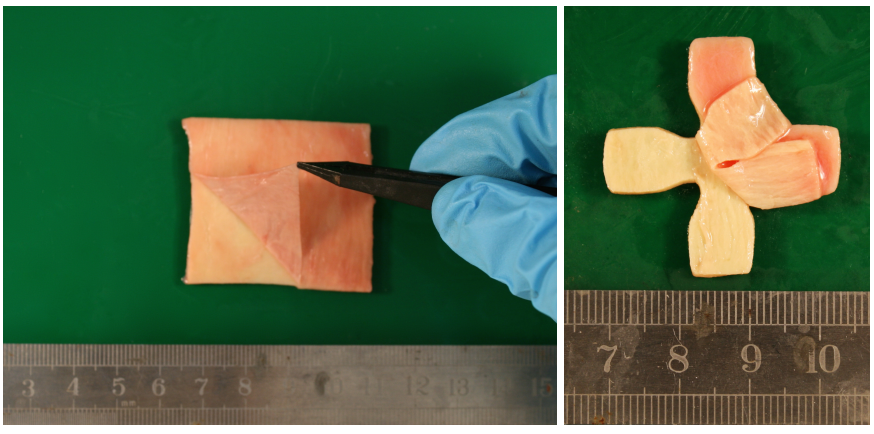

(a) Intima was pealed off carefully using forceps (Sample ID: A06)

(b) Pealing of the adventitial layer (Sample ID: A11)

Figure 3.4: Layer separation process for square shaped (a) and cruciform specimen (b).

For the cruciform specimen the customized stamping device was used to give the specimen its final shape. The individual layers were pealed off in the same way as described above (see Fig. 3.4 (b)). To all of the four arms of the cruciform specimen a piece of black sandpaper was glued, each containing three holes to make the insert of the hooks possible. Three hooks were placed on each side connected through suture. In this way the tissue was connected directly to the sandpaper via superglue but only indirectly to the hooks via the sandpaper which made attachment and mounting without harming the specimen also for the more fragile layers possible (see Fig. 3.5 (a)). Again, a thin layer of tissue marker was applied with an airbrush for subsequent particle tracking.

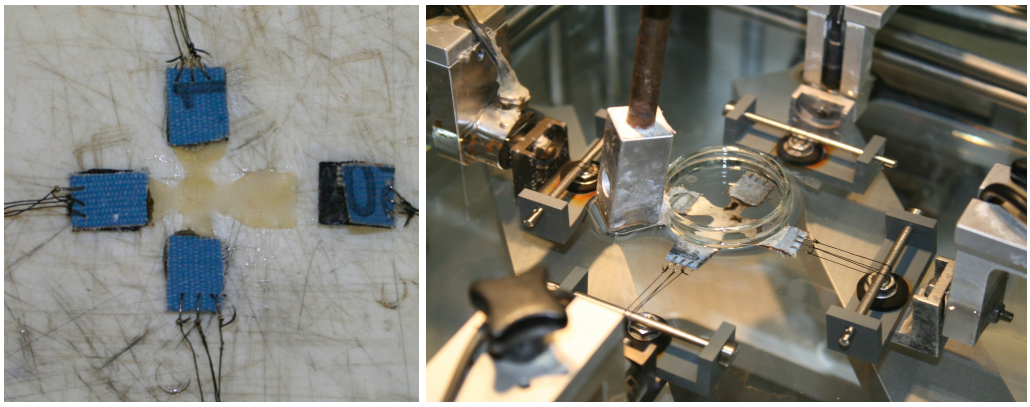

(a) Attachment of fisher hooks to cruciform sample

(b) Cruciform specimen mounted to the testing device

Figure 3.5: Attachment and mounting of cruciform specimen (Sample ID: A10)

Prior testing the thickness of each specimen was measured optically at three different points. The average thickness was then used for evaluation.

3.2 Methods

In the following chapter the laboratory procedures as well as the theoretical framework behind it, the equipment used and the way of data analysis is outlined.

3.2.1 Optical Clearing

In order to relate the mechanical behavior examined by the performed biaxial tensile tests to the microscopic structure of the sample the optical clearing procedure was introduced. This is necessary to make the tissue available for further histological examination. For the clearing procedure a small rectangular shaped piece was cut out of each sample before preparing the individual specimen making sure that the longer side marked the axial direction. After rinsing the piece twice with PBS solution the five steps of dehydration were performed, where a graded ethanol series (50%, 70%, 95%, 100% twice) was used with each step lasting 30 minutes. The dehydrated tissue was then placed in a 1:1 ethanol:BABB-solution for 4 hours. All of the clearing procedure steps occured at room temperature. The tissue was stored in 100%-BABB (a 1:2-solution of benzyl alcohol and benzyl benzonate) for at least 12 hours wraped in aluminium foil. However, the analysis of the histological structure of the samples was not part of this thesis.

3.2.2 Experimental Setup

The biaxial tensile testing device (see Fig. 3.6 (a)) was developed by the Institute of Biomechanics, University of Technology Graz, Austria, in cooperation with the company Messphysik, Fürstenfeld, Austria, for the purpose of testing soft biological and artificial tissue.

The device generally consists of:

- Four linear drives:
  The high resolution (1 µm) drives, two in x- and two in y-direction respectively, with a maximum travel range of 50 mm hold the load cells, which in turn are connected to the clamping device. The force measurement range of the individual sensors leads upto 100 N with a resolution of 0.6 mN.

- Fluid reservoir:
  Ajustable in height and made out of safety glas it serves as medium bath including a heating circuit to provide a temperature controlled environment for the specimen.

- Optical detection system:
  The videoextensometer makes biaxial non-contact stretch measurements possible.
- Computer-based data acquisition [26]

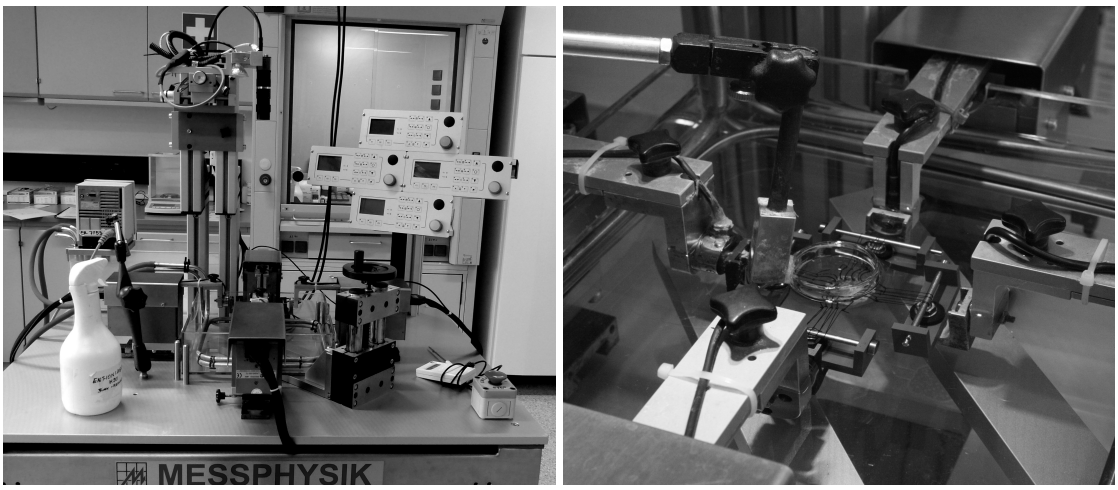

(a) Biaxial apparatus.

(b) High-angle shot of specimen mounted into the testing device with petri dish placed above

Figure 3.6: Experimental Setup for biaxial testing at the Institute of Biomechanics, University of Technology Graz, Austria.

The mounting of the specimen to the clamping device, namely twistable bars, occured in a trampoline fashion using surtures taking care to not expose the specimen to additional stretching as the tissue might be damaged (for schematic representation see Fig. 3.7). The specimen, which remains in a bath of PBS solution kept at 37°C throughout the whole testing procedure in order to provide a physiological environment, was then placed central to enable linear traction of forces. To limit interferences of the optical detection system a petri dish was positioned over the specimen to keep the area and solution above clean (see Fig. 3.6 (b)). These interferences can be caused by dissolved fat due to the heated solution and air bubbles floating around the surface.

After the calibration of the videoextensometer the starting position of the four linear drives could be determined, making sure that the specimen was exposed to proper preloading (approximately 0.01 N). As the linear drives in x- and y- direction travel away from each other the specimen experienced deformation. In order to resist this deformation the tissue exerted forces which were recorded by the load cells.

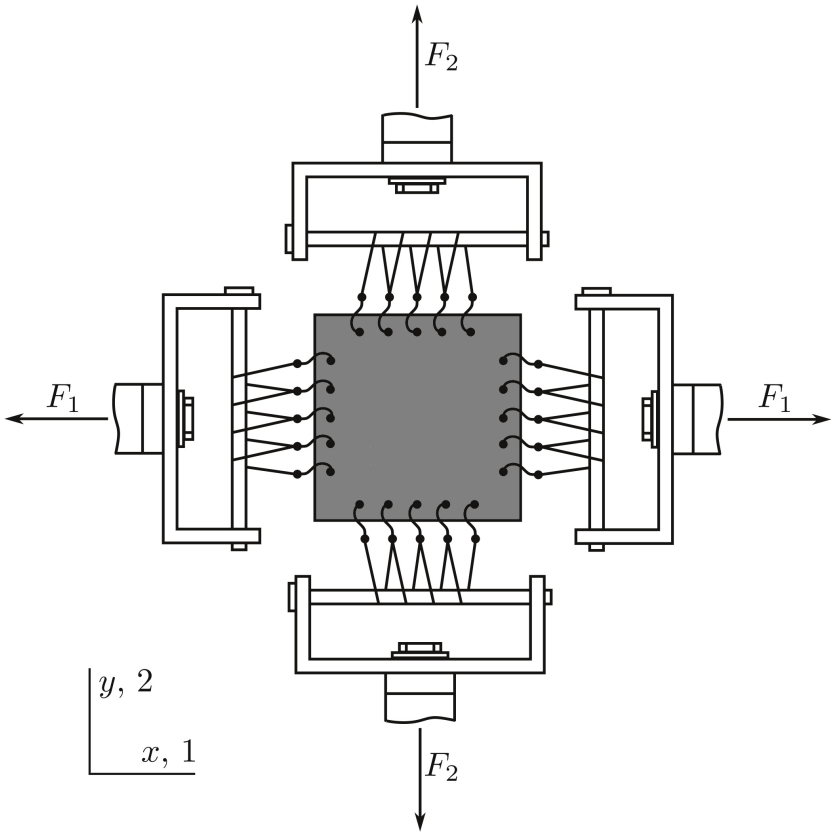

Figure 3.7: Schematic drawing of biaxial tensile test with square shaped specimen. Modified from [25].

3.2.3 Testing Protocoll

Stretch controlled tests were carried out at a testing speed of 3 mm/min considering quasi-static deformation. Different stretch levels (5%, 7.5%,10%, 12.5%, 15% and in later experiments up to 30% in steps of 2.5% to experience non-linear stiffening of the arterial tissue) are applied consecutively starting at the lowest stretch. For each stretch level five measuring cycles were performed testing the specimen at different loading ratios (1(axial direction):1(circumferential direction), 1:0.75, 1:0.5, 0.75:1, 0.5:1) to capture the anisotropic material response completely. In turn each measuring cycle is composed of a loading curve and an unloading curve. Four preconditioning cycles were performed before the measuring cycles at each stretch level. The specimen was kept in PBS solution at 37°C providing a temperature controlled testing environment. The forces applied by the loadings cells, the position of the carriages and the distance between the tracking points at an unloaded state were registered and saved in an excel sheet and later used for data analysis.

3.2.4 Data Evaluation

The data received from the performed measurements was analysed through a MATLAB (2010b, The Mathworks, Inc., Massachusetts, United States) code making computation, smoothing and plotting of the calculated data possible. To be able to evaluate the results plots were generated showing the computed cauchy-stress as a function of the stretch. This was done for each specimen at different stretch levels and loading ratios. Due to potential artifacts from the load cells and relatively high magnitudes of the residual stresses of surtures in comparison to calculated stress-stretch components the genereated plots were very noisy [27]. Smoothing of the data in form of a moving average filter was necessary (see Fig. 3.8 for the comparison of a smoothed and unsmoothed plot). The stress-stretch curves were split in an ascending and descending part and smoothed seperately making sure that the maximum value is not falsified. The obtained plots showed only little hysteresis due to the non-viscoelastic behavoir of the tissue. Hence, it is sufficient to only plot the ascending part of the curve for further analysis.

Theoretical Framework

Test control and data acquisition was done by the Software Test & Motion, DOLI, München, Germany, with the output yielding the following quantities: The two stretch ratios (λ_1, λ_2) and the applied forces (f_1,f_2) for each direction (axial direction (1) and circumferential direction (2)). The thickness T of the tissue was measured optically prior testing (reference configuration) and the specimen geometry was known (X_1, X_2).

The cauchy stress is referred to as the actual force divided by the current area and can be defined as follows (see eq. 3.1):

$$\begin{aligned} \sigma_{11} &= \frac{f_1}{t \cdot x_2} \\ \sigma_{22} &= \frac{f_2}{t \cdot x_1}\,, \end{aligned} \tag{3.1}$$

where x_1, x_2 stand for the specimen geometry in the deformed configuration, f_1, f_2 for the applied loads and t is equal to the current thickness of the specimen. Assuming incompressibility for the aortic tissue greatly simplfies the analysis of stress and strain as the deformation in radial direction is fully determined by the deformation in axial and circumferential direction [28]. Thus, the thickness t of the tissue in deformed configuration can be replaced by eq. 3.2. $X_1 = X_2$ equals 20 mm for squared shaped specimen and 5 mm for cruciform specimen (unloaded state), whereas x_1 and x_2 define the geometry at a loaded state. T stands for the initial thickness of the specimen.

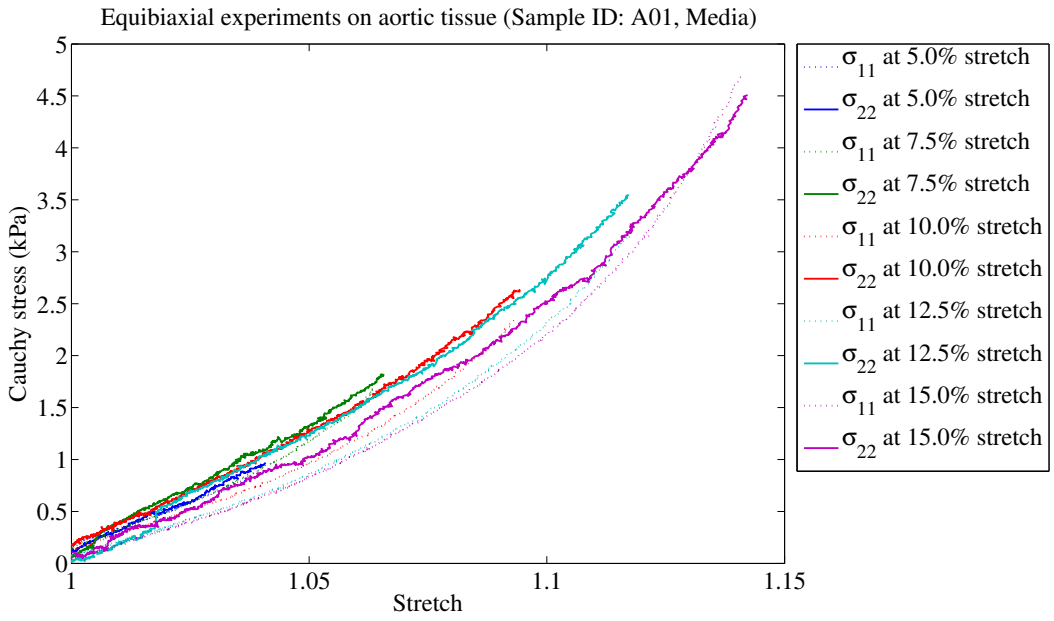

(a) Unsmoothed and noisy curve.

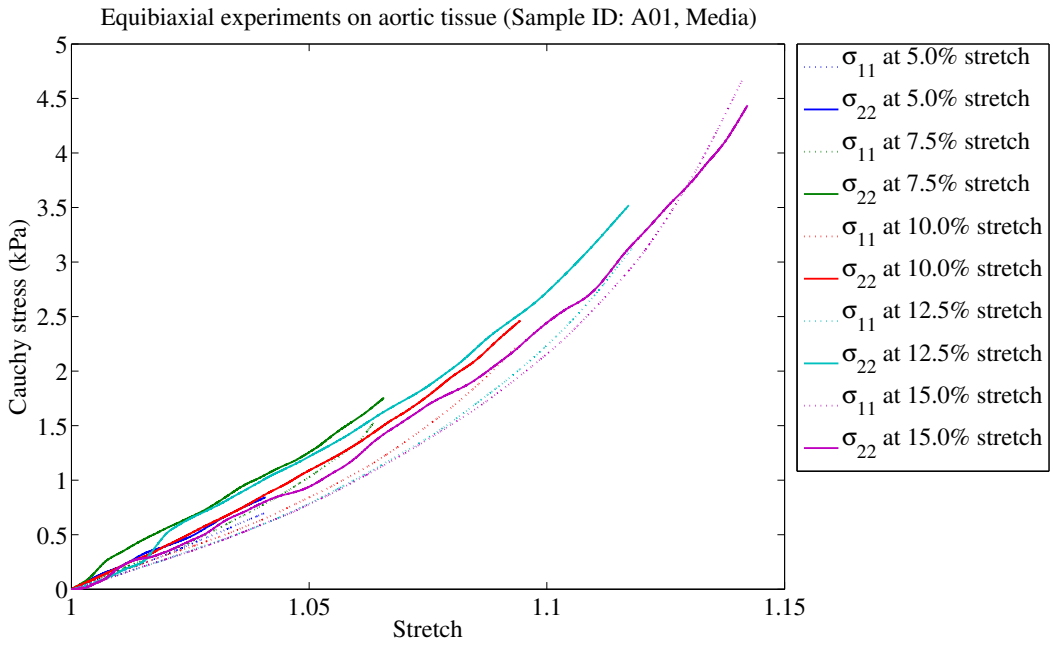

(b) Smoothed curve using an moving average filter.

Figure 3.8: Comparison of unsmoothed and smoothed stress-stretch data of the media (Sample ID: A01).

$$t = \frac{T \cdot X_1 \cdot X_2}{x_1 \cdot x_2} \tag{3.2}$$

As the stretches (λ_1, λ_2) were defined as follows (see eq. 3.3)

$$\begin{aligned} \lambda_1 &= \frac{x_1}{X_1} \\ \lambda_2 &= \frac{x_2}{X_2}\,, \end{aligned} \tag{3.3}$$

inserting eq. 3.2 and eq. 3.3 into eq. 3.1 yields the equation beneath for the cauchy stresses in axial (σ_{11}) and circumferential direction (σ_{22}):

$$\begin{aligned} \sigma_{11} &= \frac{f_1 \cdot \lambda_1}{T \cdot X_2} \\ \sigma_{22} &= \frac{f_2 \cdot \lambda_2}{T \cdot X_1}\,. \end{aligned} \tag{3.4}$$

Quantification of the Strain Field

The homogeneity of the strain field within the central region of the specimen was quantified according to [24] using a MATLAB Code, [25] to verify that the data obtained from biaxial tests is meaningful. The analysis relies on the recorded marker positions by which the particle displacements ($u_1^{(n)}$, $u_2^{(n)}$) are calculated (Laser Speckle Extensomenter, Messphysik, Fürstenfeld, Austria).

To be able to calculate the whole displacement field of the central region of the specimen mapping occured by means of shape functions (see eq. 3.5), transforming the position of the particles underlying the tracking points ($X_1^{(n)}$, $X_2^{(n)}$) from an arbitrary coordinate system (x, y) to a defined coordinate system (r, s) (see Fig. 3.9 and eq. 3.6). [24], [25]

$$
\begin{aligned}
f^{(1)}(r,s) &= \frac{1}{4}(1+r)(1+s) - \frac{1}{2}f^{(5)} - \frac{1}{2}f^{(8)} - \frac{1}{4}f^{(9)} \\
f^{(2)}(r,s) &= \frac{1}{4}(1-r)(1+r) - \frac{1}{2}f^{(5)} - \frac{1}{2}f^{(6)} - \frac{1}{4}f^{(9)} \\
f^{(3)}(r,s) &= \frac{1}{4}(1-r)(1-s) - \frac{1}{2}f^{(6)} - \frac{1}{2}f^{(7)} - \frac{1}{4}f^{(9)} \\
f^{(4)}(r,s) &= \frac{1}{4}(1+r)(1-s) - \frac{1}{2}f^{(7)} - \frac{1}{2}f^{(8)} - \frac{1}{4}f^{(9)} \\
f^{(5)}(r,s) &= \frac{1}{2}(1-r^2)(1+s) - \frac{1}{2}f^{(9)} \\
f^{(6)}(r,s) &= \frac{1}{2}(1-s^2)(1-r) - \frac{1}{2}f^{(9)} \\
f^{(7)}(r,s) &= \frac{1}{2}(1-r^2)(1-s) - \frac{1}{2}f^{(9)} \\
f^{(8)}(r,s) &= \frac{1}{2}(1-s^2)(1+r) - \frac{1}{2}f^{(9)} \\
f^{(9)}(r,s) &= (1-r^2)(1-s^2)
\end{aligned}
\tag{3.5}
$$

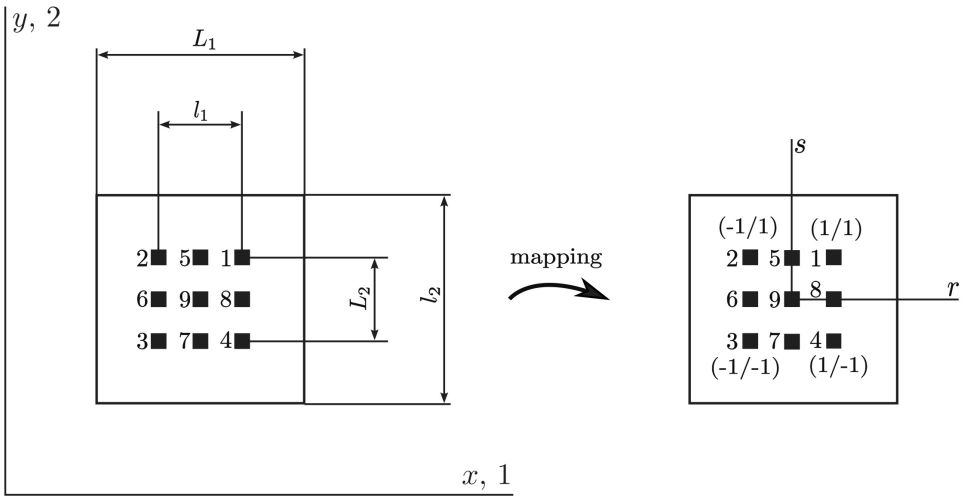

Figure 3.9: Schematic diagram of mapping from an arbitrary coordinate system (x,y) into an isoparametric coordinate system (r,s). Taken from [25].

$$
X_1(r,s) = \sum_{n=1}^{9} f^{(n)}(r,s) X_1^{(n)} \qquad X_2(r,s) = \sum_{n=1}^{9} f^{(n)}(r,s) X_2^{(n)} \tag{3.6}
$$

The displacements in r- and s-direction were obtained as follows:

$$u_1(r,s) = \sum_{n=1}^{9} f^{(n)}(r,s)u_1^{(n)} \qquad u_2(r,s) = \sum_{n=1}^{9} f^{(n)}(r,s)u_2^{(n)} \tag{3.7}$$

Strains were obtained by performing partial derivatives of displacements and had to be mapped back to the x,y coordinate system (see eq. 3.8). Under the incompressibility assumption the deformation gradient (F) could be calculated (see eq. 3.9). [24], [25]

$$\begin{bmatrix} \frac{\partial u_1}{\partial X_1}(r,s) \\ \frac{\partial u_1}{\partial X_2}(r,s) \end{bmatrix} = J^{-1} \begin{bmatrix} \frac{\partial u_1}{\partial r} \\ \frac{\partial u_1}{\partial s} \end{bmatrix} \qquad \begin{bmatrix} \frac{\partial u_2}{\partial X_1}(r,s) \\ \frac{\partial u_2}{\partial X_2}(r,s) \end{bmatrix} = J^{-1} \begin{bmatrix} \frac{\partial u_2}{\partial r} \\ \frac{\partial u_2}{\partial s} \end{bmatrix} \tag{3.8}$$

$$F = \begin{bmatrix} \lambda_1 & \gamma_1 \\ \gamma_2 & \lambda_2 \end{bmatrix} = \begin{bmatrix} 1 + \frac{\partial u_1}{\partial X_1} & \frac{\partial u_1}{\partial X_2} \\ \frac{\partial u_2}{\partial X_1} & 1 + \frac{\partial u_2}{\partial X_2} \end{bmatrix} \tag{3.9}$$

Statistical Analysis of Results

In order to be able to interpret differences in the obtained results and make a sufficient comparison descritive statistics was used. Because of the small sample size (only 11 samples tested) it could not be assumed that the distribution of the results is gaussian. Hence, the usage of the mean and standard deviation would not be conclusive. The determination of the median and interquartile ranges seemed to be more suitable, supplying a more meaningful outcome. The median (for data that has been put in order) can be calculated as follows (see eq. 3.10 for an uneven number of data points (n) and eq. 3.11 when n equals an even number):

$$\tilde{x} = x_{(n+1)/2} \tag{3.10}$$

$$\tilde{x} = \frac{1}{2}(x_{\frac{n}{2}} + x_{\frac{n}{2}+1})\,. \tag{3.11}$$

The interquartile range can be determined by subtracting the first quartile (Q1 = Q_{25}) from the third quartile ((Q3 = Q_{75}). The first quartile stands for the value below which 25% of all observations fall and the third quartile for the value below which 75% of all observations fall. Percentile (Q_p) is the more general expression for a quartile (see eq. 3.12). [29]

$$Q_p = \begin{cases} x_{(k)} & \text{for n} \cdot \text{p is no integer } (k = int(n \cdot p) + 1) \\ \frac{1}{2}(x_{(k)} + x_{(k+1)}) & \text{for n} \cdot \text{p is an integer } (k = n \cdot p) \end{cases} \tag{3.12}$$

Outliers can be detected and rated as minor (see eq. 3.13) or major (see eq. 3.14) through classification into one of the following intervalls [29]:

$$\begin{aligned} x_i &\geq Q_{75} + 1.5 \cdot IQR \\ x_i &\leq Q_{25} - 1.5 \cdot IQR \end{aligned} \tag{3.13}$$

$$\begin{aligned} x_i &\geq Q_{75} + 3 \cdot IQR \\ x_i &\leq Q_{25} - 3 \cdot IQR\,. \end{aligned} \tag{3.14}$$

All calculation were carried out using R (R Foundation for Statistical Computing, Vienna, Austria). Further, Whisker boxplots and stripcharts were generated for the purpose of visualisation.

3.2.5 Restricting Factors

Several factors may have an influence on the mechanical behavior of the tissue and therefore falsify the results obtained.

Temperature Change

Aiming for an environment for the specimen that is as physiological as possible the standard temperature for mechanical testing of arteries is 37°C. All tests were carried out at this temperature. Nevertheless, it is known that temperature fluctuations can significantly change the mechanical response of the tissue. A cool down of the temperature by only 1°C causes an stiffness increase of approximately 5% (see Fig. 3.10). [30], [31]

Specimen Conservation

As most of the samples were frozen at -20°C for a different amount of time (see Tab. 3.2) and thawed (at 4°C) prior specimen preparation the influence of this conservation method on the mechanical properties is of interest. However, hardly any relevant studies could

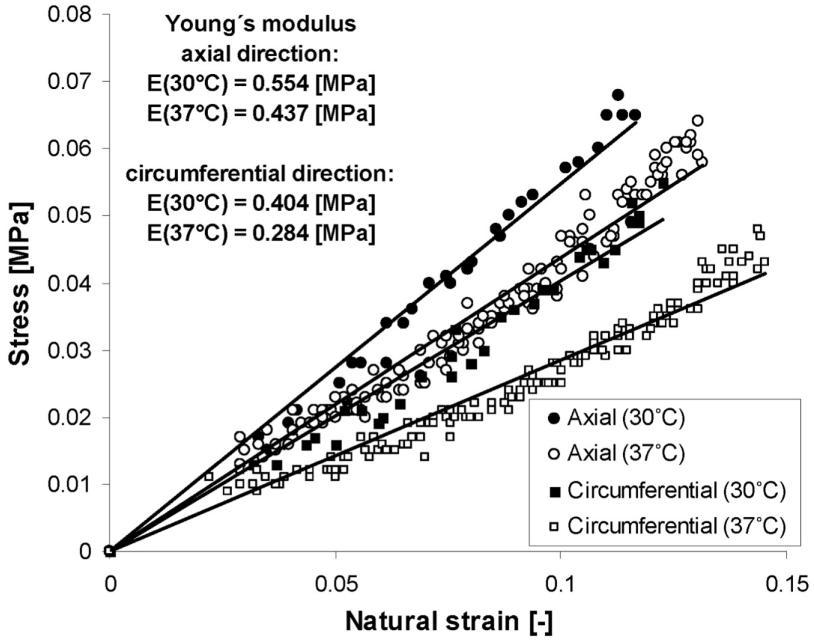

Figure 3.10: Stress-natural strain diagram of arteries tested at different temperatures. The stress-natural strain response is significantly stiffer at a temperature of 30°C than at 37°C. Taken from [30].

be found in literature about the effects of freezing besides displaying mostly a contrary outcome. [30] showed that between specimen tested within two hours of ectomy and specimens frozen over night (at -20°C for approximately 12 hours) no significant changes in the mechanical properties could be reported and therefore the effects of the freezing process can be classified as negligible. Similar results where obtained by [32] with samples frozen over a period of three month. Arbitrarily, [33] reported that freezing (at -20°C for 2 or 5 minutes) causes a change in the stress-strain properties, especially in the toe region. The change of the mechanical properties may be explained by the loss of smooth muscle cell viability, damage to the extra cellular matrix, bulk redistribution of water or variations in the alignment [33]. The conservation time of most of the samples used in this study clearly exceeds 3 month lasting upto almost three years for some and varies strongly within the rest. Hence, it was not possible to make a valid statement about the effects of freezing furthermore because of the lacking data of freshly tested samples. Anyhow, some of the samples showed a brittle character after being frozen bringing up the assumption that the freezing process does have an influence on the mechanical properties suggesting to focus more on the conservation method in ongoing studies.

Table 3.2: Overview of amount of time the samples had been frozen prior testing due to conservation purposes.

Sample ID	Date frozen	Date tested	# days frozen
A02	04.12.2014	15.12.2014	11
A02	02.11.2014	18.12.2014(M,C),18.06.2015(A)	46(M,C),228(A)
A03	12.04.2012	04.02.2015(M),06.02.2015(A,C)	1028(M),1030(A,C)
A04	28.08.2013	12.02.2015(M),16.02.2015(A,C)	533(M),537(A,C)
A05	09.07.2012	06.03.2015	970
A06	19.07.2014	27.03.2015	251
A07	30.10.2013	10.04.2015	527
A08	23.04.2015	04.05.2015	11
A09	17.05.2015	01.06.2015	15
A10	27.09.2012	17.06.2015	933
A11	01.07.2015	20.08.2015	50

Preconditioning

Arteries tend to soften when exposed to multiple measuring cycles. After a certain number of loading and unloading cycles a repeatable cyclic behavior is exhibited. This process is called preconditioning. [1]

[30] reported an insignificant influence of preconditioning up to a stretch level of 35% for equibiaxial tension test. On the contrary in the first few cycles of planar and uniaxial tension test the effect of stress softening becomes clearly visible, which may be caused by an alignment of collagen fibres in the direction of the applied load [30]. In this study four preconditioning cycles were performed before the measuring cycles at each stretch level.

4 Results

The results of the biaxial tensile tests of the abdominal aorta are shown and compared in the following chapter. Comparisons were made in terms of different age groups of donors, gender, specimen geometry and the individual layers at varying stretch levels.

4.1 Age-related Mechanical Behavior

Based on [34] samples could be divided into two age groups. Samples A02, A08 and A10 fall into the group up to 60 years of age, whereas samples A01, A03, A04-A07, A09 and A11 fall into the group above 60 years of age. The median and the IQR of the maximum Cauchy stresses of each age group are summarised in Tab. 4.1 for the media, in Tab. 4.2 for the adventitia and in Tab. 4.3 for the composite at stretch levels 5%, 7.5%, 10.0%, 12.5% and 15%. The number of data points n used for the calculations of the median an IQR varied between age groups, layers and stretch levels.

Table 4.1: Comparison of equibiaxial mechanical behavior of the media in relation to age. Median and IQR [Q1; Q3] of maximum Cauchy stresses are shown for the two age groups at different stretch levels. The number of data points n used for the calculations of the median and IQR varies between age groups and stretch levels.

Stretch	Age ≤ 60					Age >60				
$\lambda_1 = \lambda_2$	n	σ_{11}		σ_{22}		n	σ_{11}		σ_{22}	
		$\tilde{x}$ (kPa)	IQR (kPa)	$\tilde{x}$ (kPa)	IQR (kPa)		$\tilde{x}$ (kPa)	IQR (kPa)	$\tilde{x}$ (kPa)	IQR (kPa)
1.050	3	0.59	[0.47; 0.77]	1.19	[0.91; 1.23]	8	0.65	[0.47; 0.89]	1.21	[0.85; 1.38]
1.075	3	1.12	[0.84; 1.20]	2.05	[1.55; 2.12]	8	1.06	[0.83; 1.43]	1.73	[1.61; 2.07]
1.100	3	1.61	[1.21; 1.84]	3.13	[2.28; 3.23]	7	1.48	[1.30; 2.01]	2.46	[2.20; 2.78]
1.125	2	1.62	[1.35; 1.89]	2.86	[2.41; 3.30]	6	2.51	[1.76; 3.22]	3.76	[3.41; 4.02]
1.150	3	2.52	[1.95; 3.27]	4.06	[3.25; 4.96]	6	3.62	[2.43; 5.08]	4.92	[4.45; 5.68]

Fig. 4.1 and Fig. 4.2 show the mechanical behavior in terms of maximum Cauchy stresses in relation to age as Whisker boxplots and corresponding stripcharts at stretches of 5% and 15% in axial and circumferential direction. Further, the Cauchy stress vs. stretch diagrams of the composite of sample A02 (donor 45 years of age) and A03 (donor 82 years of age) are shown (see Fig. 4.3). A comparison in terms of a stress vs. stretch diagram was not made for the media and adventitia as these layers ruptured at a stretch level of 10% and 12.5% for sample A03.

Table 4.2: Comparison of equibiaxial mechanical behavior of the adventitia in relation to age. Median and IQR [Q1;Q3] of maximum Cauchy stresses are shown for the two age groups at different stretch levels for a varying number of data points n.

Stretch	Age ≤ 60					Age >60				
$\lambda_1 = \lambda_2$	n	σ_{11}		σ_{22}		n	σ_{11}		σ_{22}	
		$\tilde{x}$ (kPa)	IQR (kPa)	$\tilde{x}$ (kPa)	IQR (kPa)		$\tilde{x}$ (kPa)	IQR (kPa)	$\tilde{x}$ (kPa)	IQR (kPa)
1.050	3	0.21	[0.15; 0.26]	0.38	[0.25; 0.39]	8	0.12	[0.08; 0.25]	0.16	[0.11; 0.25]
1.075	3	0.32	[0.22; 0.35]	0.54	[0.36; 0.63]	6	0.13	[0.10; 0.25]	0.22	[0.17; 0.29]
1.100	3	0.52	[0.33; 0.57]	0.76	[0.52; 0.82]	7	0.28	[0.17; 0.34]	0.34	[0.29; 0.49]
1.125	3	0.63	[0.43; 0.82]	1.02	[0.70; 1.10]	5	0.23	[0.21; 0.33]	0.41	[0.39; 0.53]
1.150	3	0.85	[0.59; 1.12]	1.28	[0.92; 1.47]	5	0.47	[0.31; 0.51]	0.65	[0.59; 0.94]

Table 4.3: Comparison of equibiaxial mechanical behavior of the composite in relation to age. Median and IQR [Q1; Q3] of maximum Cauchy stresses are shown for the two age groups at different stretch levels for a varying number of data points n.

Stretch	Age ≤ 60					Age >60				
$\lambda_1 = \lambda_2$	n	σ_{11}		σ_{22}		n	σ_{11}		σ_{22}	
		$\tilde{x}$ (kPa)	IQR (kPa)	$\tilde{x}$ (kPa)	IQR (kPa)		$\tilde{x}$ (kPa)	IQR (kPa)	$\tilde{x}$ (kPa)	IQR (kPa)
1.050	3	1.02	[0.72; 2.32]	1.68	[1.16; 2.20]	8	0.55	[0.34; 0.78]	0.59	[0.45; 0.74]
1.075	3	2.46	[1.58; 2.96]	3.27	[2.13; 3.30]	7	0.60	[0.45; 0.97]	0.90	[0.61; 1.27]
1.100	2	2.49	[1.73; 3.24]	2.84	[2.13; 3.56]	7	1.33	[0.64; 1.58]	1.38	[0.80; 2.44]
1.125	2	3.38	[2.36; 4.40]	3.89	[2.89; 4.90]	6	0.87	[0.58; 1.51]	1.26	[1.02; 1.67]
1.150	2	3.83	[2.77; 4.89]	4.50	[3.44; 5.56]	5	1.50	[0.94; 2.11]	1.81	[1.47; 2.37]

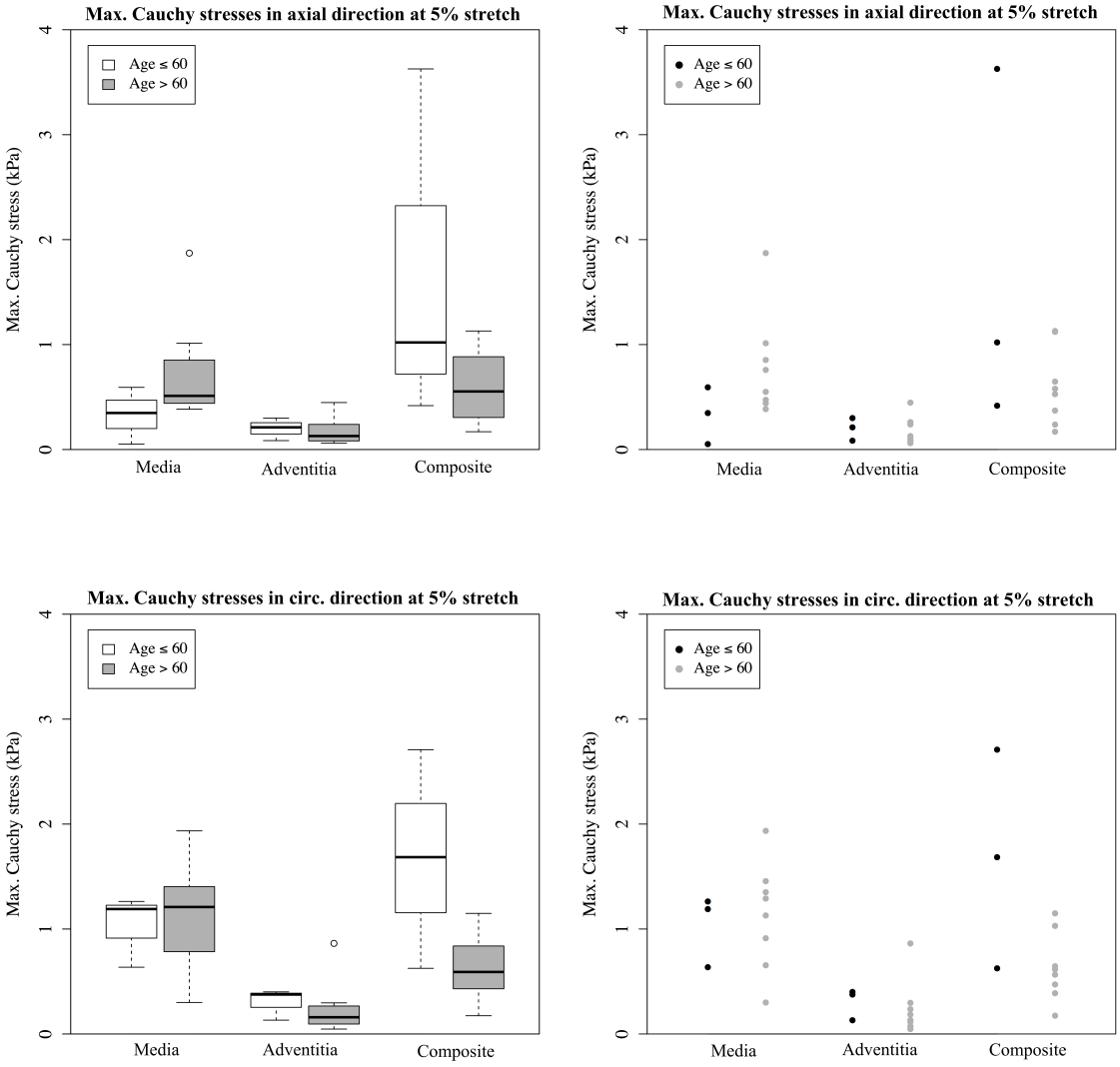

Figure 4.1: Mechanical behavior in terms of maximum Cauchy stresses for the media, adventitia and the composite in relation to age. The maximum Cauchy stresses at 5% stretch in axial direction and circumferential direction are shown. On the left hand side Whisker boxplots are presented, where values of the age group up to 60 years of age are marked in white, while values of the age group above 60 years are marked in grey. On the right hand side the corresponding stripcharts are shown, displaying the individual data points of the younger age group in black and data points of the age group above 60 years in grey.

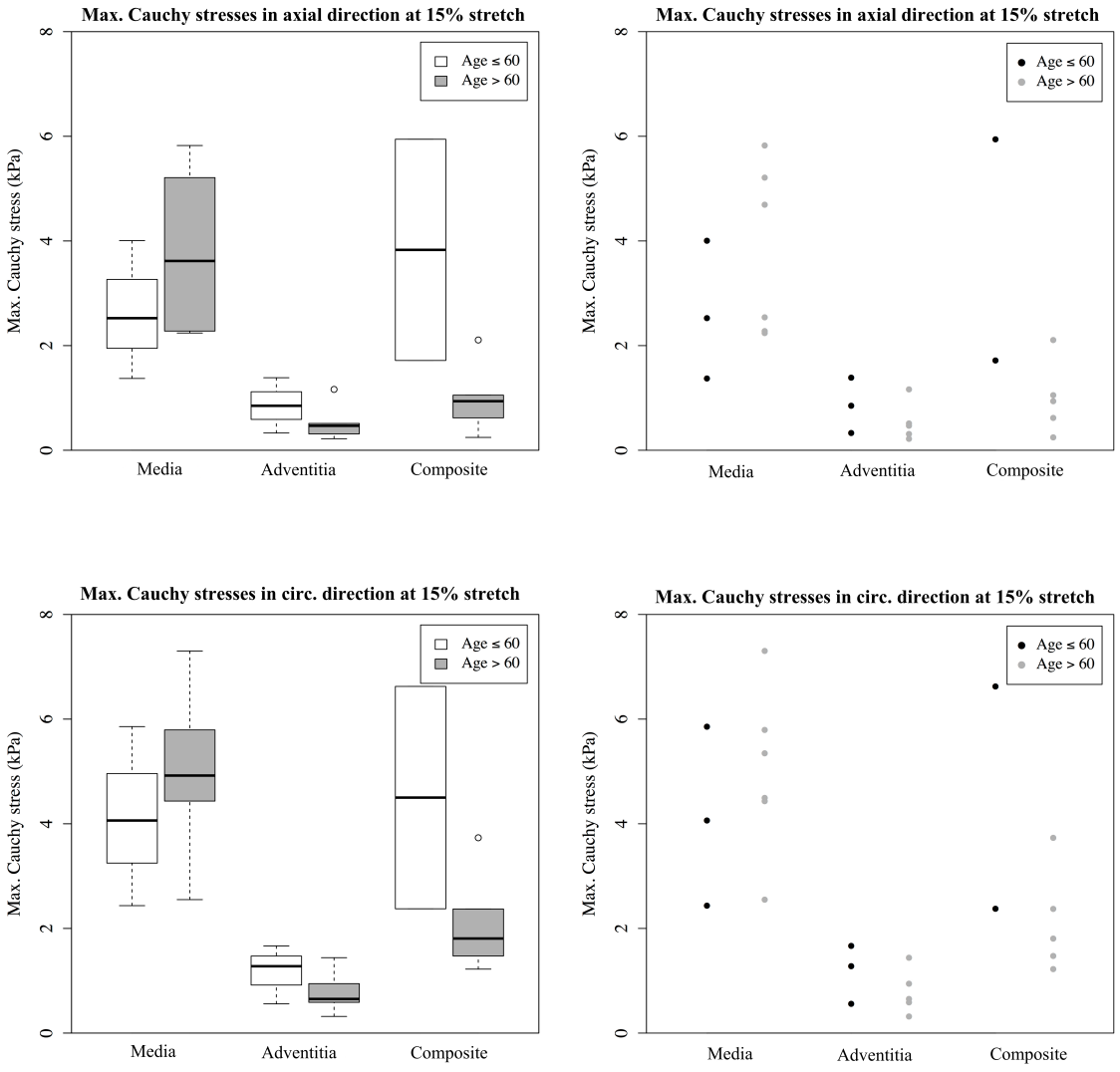

Figure 4.2: Mechanical behavior in terms of maximum Cauchy stresses for the media, adventitia and the composite in relation to age. The maximum Cauchy stresses at 15% stretch in axial direction and circumferential direction are shown. On the left hand side Whisker boxplots are presented, where values of the age group up to 60 years of age are marked in white, while values of the age group above 60 years are marked in grey. On the right hand side the corresponding stripcharts are shown, displaying the individual data points of the younger age group in black and data points of the age group above 60 years in grey.

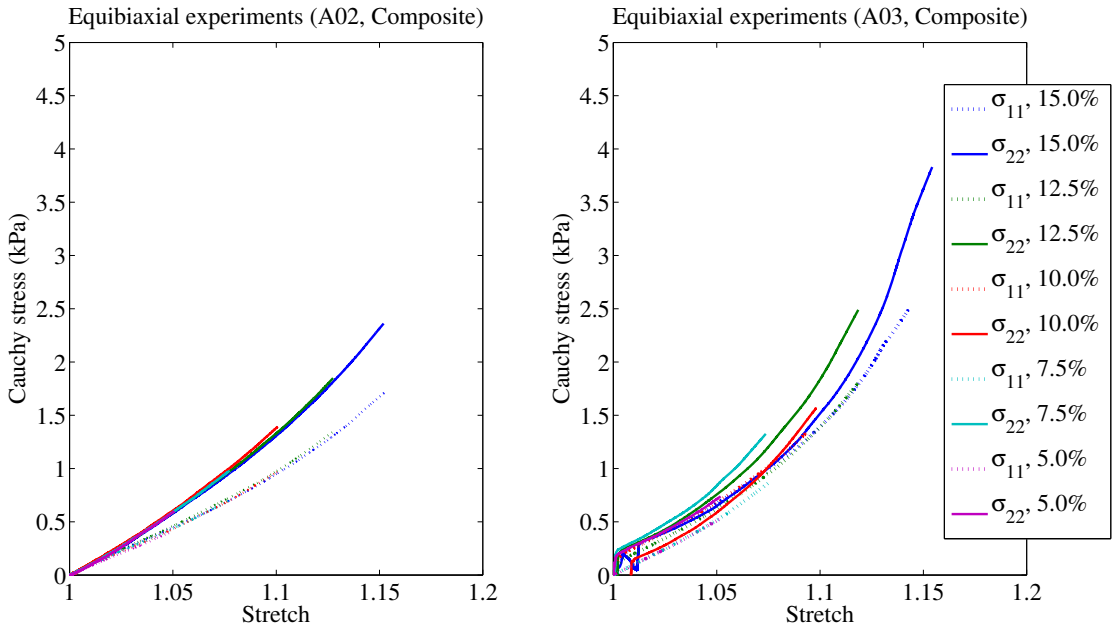

Figure 4.3: Stress vs. stretch diagrams of composite of samples A02 (left) and A03 (right) comparing the age related mechanical behavior of the tissue at a stretch level of 5%, 7.5%, 10%, 12.5% and 15% in axial (σ_{11}) and cirumferential direction (σ_{22}). Sample A02 originated from a donor aged 45 belonging to the age group up to sixty years of age, while sample A03 belongs to the the age group above 60 years of age with donor aged 82.

4.2 Gender-dependent Mechanical Behavior

Samples A01, A03, A04 and A07 (orginating from male donors) were compared with Samples A05, A06, A09 (originating from female donors). All samples fall within the same age group (above 60 years of age) and show the same sample geometry (20x20 mm). The median and the IQR of the maximum Cauchy stresses for each gender are summarised in Tab. 4.4 for the media, in Tab. 4.5 for the adventitia and in Tab. 4.6 for the composite at stretch levels 5%, 7.5%, 10.0%, 12.5% and 15%. The number of data points n used for the calculations of the median and IQR varied between genders, layers and stretch levels. Fig. 4.4 and Fig. 4.5 show the mechanical behavior in terms of maximum Cauchy stresses in relation to the gender of the donor as Whisker boxplots and corresponding stripcharts at stretches of 5% and 15% in axial and circumferential direction.

Table 4.4: Comparison of equibiaxial mechanical behavior of the media in relation to the gender of the donor. Median and IQR [Q1; Q3] of maximum Cauchy stresses are shown for the two genders at different stretch levels. The number of data points n used for the calculations of the median and IQR varied between genders and stretch levels.

Stretch	male					female				
$\lambda_1 = \lambda_2$	n	σ_{11}		σ_{22}		n	σ_{11}		σ_{22}	
		$\tilde{x}$ (kPa)	IQR (kPa)	$\tilde{x}$ (kPa)	IQR (kPa)		$\tilde{x}$ (kPa)	IQR (kPa)	$\tilde{x}$ (kPa)	IQR (kPa)
1.050	4	0.70	[0.51; 1.11]	1.24	[0.92; 1.50]	3	0.47	[0.46; 0.62]	0.91	[0.78; 1.10]
1.075	4	1.25	[0.83; 2.22]	1.97	[1.52; 2.90]	3	1.05	[0.93; 1.06]	1.71	[1.50; 1.72]
1.100	3	1.23	[1.20; 1.78]	2.46	[1.88; 2.78]	3	1.66	[1.42; 1.72]	2.29	[2.25; 2.45]
1.125	3	1.75	[1.72; 2.49]	3.50	[2.66; 3.76]	2	2.51	[2.15; 2.87]	3.70	[3.54; 3.86]
1.150	3	2.28	[2.26; 3.49]	4.50	[3.52; 4.92]	2	4.18	[3.36; 5.00]	5.87	[5.15; 6.59]

4.3 Geometry-dependent Mechanical Behavior

Maximum Cauchy stresses of Sample A09 showing a square shaped specimen geometry and maximum Cauchy stresses of sample A10 revealing a cruciform shape were examined for the media (see Tab. 4.7), the adventitia (see Tab. 4.8) and the composite (see Tab. 4.9). This was done at different stretch levels (5% upto 15% in steps of 2.5%) in axial as well as circumferential direction. To enable examination of the homogeneity of the deformation field the particle histories of the media, adventitia and composite were plotted for equibiaxial tests at 10% stretch (see Fig. 4.7). Further, sample A09 (square shape) was compared with sample A11 (cruciform) in terms of stress vs. stretch diagrams opposing the medial and adventitial layer with the composite at 10% stretch (see Fig. 4.6).

Table 4.5: Comparison of equibiaxial mechanical behavior of the adventitia in relation to the gender of the donor. Median and IQR [Q1; Q3] of maximum Cauchy stresses are shown for the two genders at different stretch levels. The number of data points n used for the calculations of the median and IQR varies between genders and stretch levels.

Stretch	male					female				
$\lambda_1 = \lambda_2$	n	σ_{11}		σ_{22}		n	σ_{11}		σ_{22}	
		$\tilde{x}$ (kPa)	IQR (kPa)	$\tilde{x}$ (kPa)	IQR (kPa)		$\tilde{x}$ (kPa)	IQR (kPa)	$\tilde{x}$ (kPa)	IQR (kPa)
1.050	4	0.09	[0.08; 0.19]	0.13	[0.07; 0.35]	3	0.13	[0.09; 0.18]	0.13	[0.12; 0.21]
1.075	2	0.11	[0.10; 0.13]	0.13	[0.11; 0.14]	3	0.13	[0.10; 0.30]	0.23	[0.22; 0.38]
1.100	3	0.28	[0.20; 0.30]	0.34	[0.26; 0.38]	3	0.19	[0.17; 0.38]	0.29	[0.29; 0.53]
1.125	2	0.26	[0.22; 0.29]	0.36	[0.28; 0.44]	3	0.23	[0.22; 0.54]	0.41	[0.40; 0.73]
1.150	2	0.34	[0.28; 0.41]	0.49	[0.40; 0.57]	3	0.51	[0.41; 0.84]	0.94	[0.77; 1.19]

Table 4.6: Comparison of equibiaxial mechanical behavior of the composite in relation to the gender of the donor. Median and IQR [Q1; Q3] of maximum Cauchy stresses are shown for the two genders at different stretch levels. The number of data points n used for the calculations of the median and IQR varies between genders and stretch levels.

Stretch	male					female				
$\lambda_1 = \lambda_2$	n	σ_{11}		σ_{22}		n	σ_{11}		σ_{22}	
		$\tilde{x}$ (kPa)	IQR (kPa)	$\tilde{x}$ (kPa)	IQR (kPa)		$\tilde{x}$ (kPa)	IQR (kPa)	$\tilde{x}$ (kPa)	IQR (kPa)
1.050	4	0.38	[0.22; 0.68]	0.48	[0.34; 0.71]	3	0.58	[0.48; 0.61]	0.62	[0.54; 0.62]
1.075	4	0.47	[0.33; 0.69]	0.91	[0.49; 1.25]	2	0.76	[0.66; 0.87]	0.77	[0.71; 0.84]
1.100	4	0.92	[0.48; 1.45]	1.25	[0.71; 2.09]	2	1.06	[0.92; 1.21]	1.11	[0.97; 1.24]
1.125	4	0.59	[0.57; 0.91]	1.06	[0.92; 1.48]	2	1.39	[1.26; 1.51]	1.58	[1.49; 0.67]
1.150	4	1.00	[0.86; 1.40]	1.64	[1.41; 2.29]	1	2.11	[2.11; 2.11]	2.37	[2.37; 2.37]

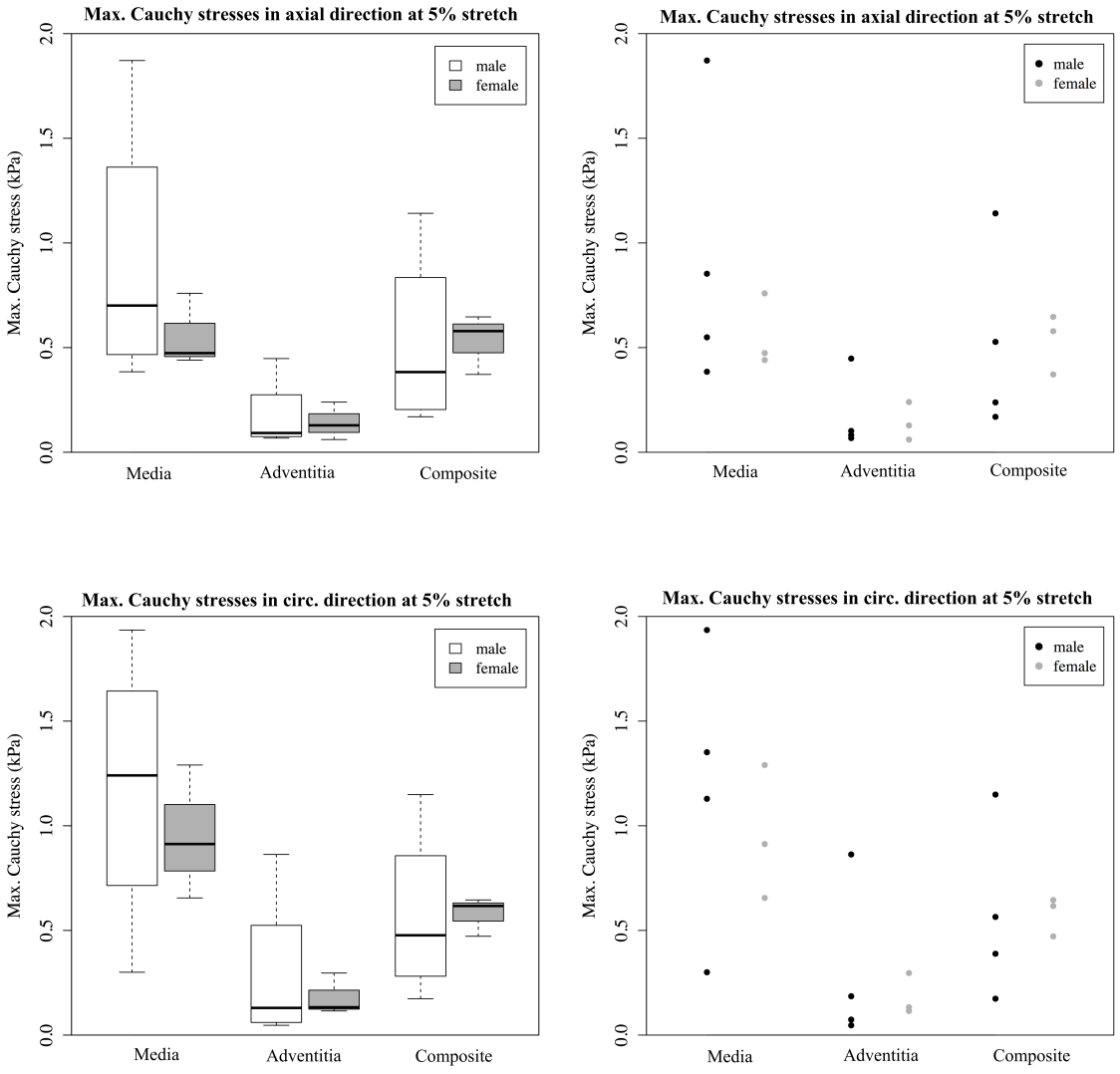

Figure 4.4: Mechanical behavior in terms of maximum Cauchy stresses for the media, adventitia and the composite in relation to the gender. The maximum Cauchy stresses at 5% stretch in axial direction and circumferential direction are shown. On the left hand side Whisker boxplots are presented, where values of the male gender are marked in white, while values of the female gender are marked in grey. On the right hand side the corresponding stripcharts are shown, displaying the individual data points of the male group in black and data points of the female group in grey.

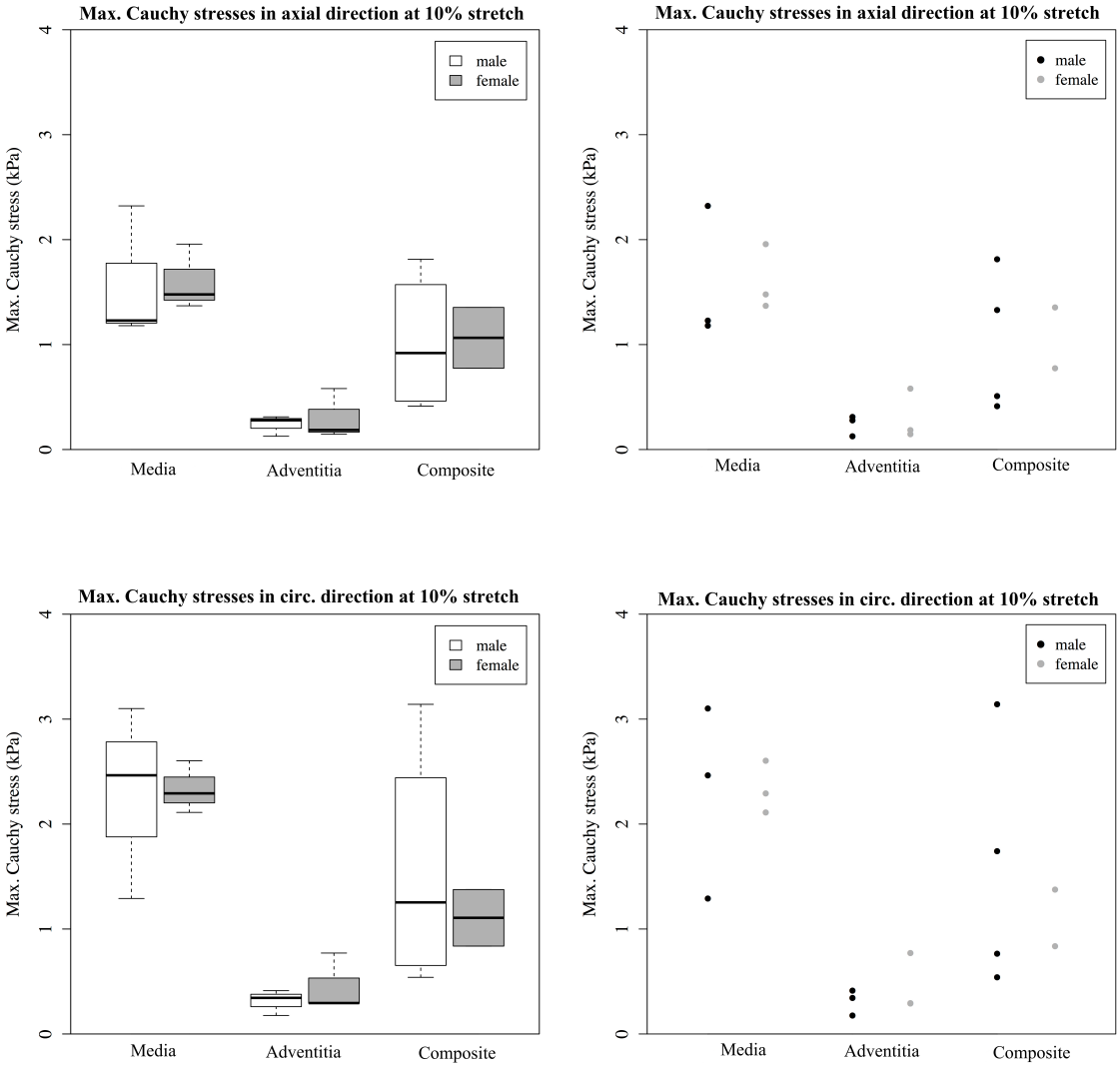

Figure 4.5: Mechanical behavior in terms of maximum Cauchy stresses for the media, adventitia and the composite in relation to the gender. The maximum Cauchy stresses at 10% stretch in axial direction and circumferential direction are shown. On the left hand side Whisker boxplots are presented, where values of the male gender are marked in white, while values of the female gender are marked in grey. On the right hand side the corresponding stripcharts are shown, displaying the individual data points of the male group in black and data points of the female group in grey.

Table 4.7: Comparison of equibiaxial mechanical behavior of the media in relation to the sample geometry for sample A09 (20x20 mm) and sample A10 (cruciform shape).

Stretch	20x20 mm		cruciform	
$\lambda_1 = \lambda_2$	σ_{11}	σ_{22}	σ_{11}	σ_{22}
	(kPa)	(kPa)	(kPa)	(kPa)
1.050	0.76	1.29	0.95	1.26
1.075	1.05	1.72	1.28	2.19
1.100	1.37	2.21	2.06	3.32
1.125	-	-	-	-
1.150	-	-	4.01	5.86

Table 4.8: Comparison of equibiaxial mechanical behavior of the adventitia in relation to the sample geometry for sample A09 (20x20 mm) and sample A10 (cruciform shape).

Stretch	20x20 mm		cruciform	
$\lambda_1 = \lambda_2$	σ_{11}	σ_{22}	σ_{11}	σ_{22}
	(kPa)	(kPa)	(kPa)	(kPa)
1.050	0.06	0.14	0.30	0.40
1.075	0.13	0.23	0.39	0.71
1.100	0.15	0.29	0.61	0.89
1.125	0.21	0.41	1.01	1.18
1.150	0.31	0.59	1.39	1.67

Table 4.9: Comparison of equibiaxial mechanical behavior of the composite in relation to the sample geometry for sample A09 (20x20 mm) and sample A10 (cruciform shape).

Stretch	20x20 mm		cruciform	
$\lambda_1 = \lambda_2$	σ_{11}	σ_{22}	σ_{11}	σ_{22}
	(kPa)	(kPa)	(kPa)	(kPa)
1.050	0.65	0.62	3.63	2.71
1.075	0.97	0.90	3.46	3.23
1.100	1.35	1.38	4.00	4.28
1.125	1.63	1.76	5.41	5.91
1.150	2.11	2.37	5.94	6.63

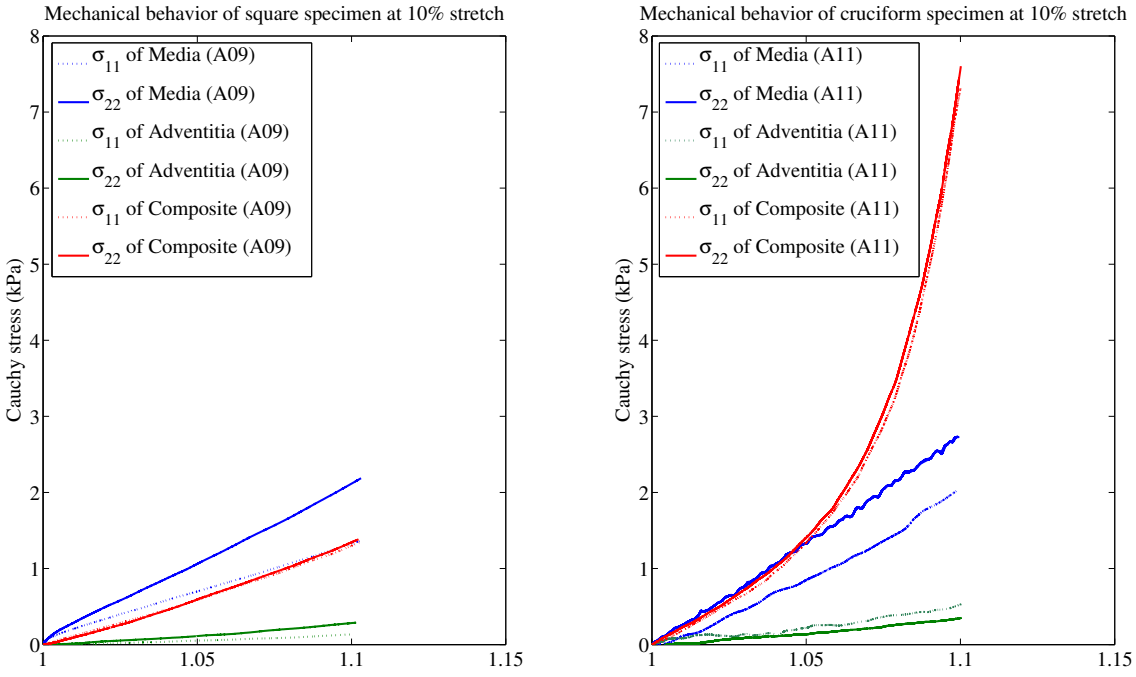

Figure 4.6: Comparison of the media, adventitia and composite in form of a stress vs. stretch diagram opposing the square shaped and cruciform specimen (Samples A09 and A11) at a stretch level of 10%.

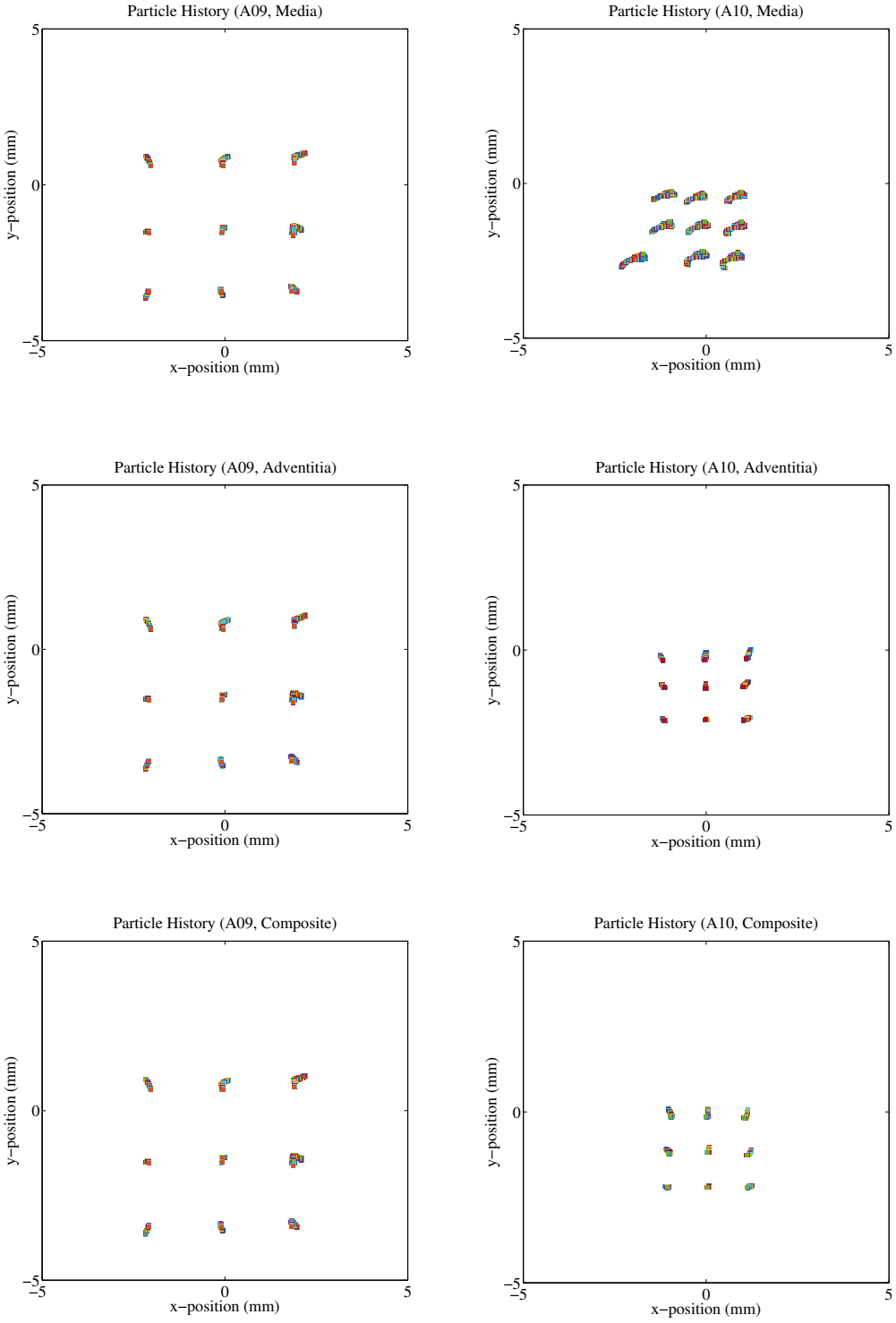

Figure 4.7: Particle History of media (top), adventitia (center) and composite (bottom) of the square shaped sample (A09) and the cruciform sample (A10) visualising the deformation in axial (x-position) and circumferntial direction (y-position) for equibiaxial experiments at 10% stretch.

4.4 Intima

Tab. 4.10 shows the maximum Cauchy stresses in axial and cirumferential direction of samples A08, A10 and A11 at different stretch levels (5% up to 15% in steps of 2.5%). Stress vs. stretch diagrams of sample A08 and sample A11 are shown in Fig. 4.8.

Table 4.10: Maximum Cauchy stresses for the intimal layer in axial and circumferential direction at different stretch levels.

Stretch	1.050		1.075		1.100		1.125		1.150	
$\lambda_1 = \lambda_2$	σ_{11} (kPa)	σ_{22} (kPa)	σ_{11} (kPa)	σ_{22} (kPa)	σ_{11} (kPa)	σ_{22} (kPa)	σ_{11} (kPa)	σ_{22} (kPa)	σ_{11} (kPa)	σ_{22} (kPa)
A08	0.67	1.29	1.41	1.96	1.77	2.69	2.72	3.57	3.3597	4.67
A10	6.58	19.68	-	-	-	-	-	-	-	-
A11	1.47	4.28	2.28	7.29	6.69	14.14	-	-	-	-

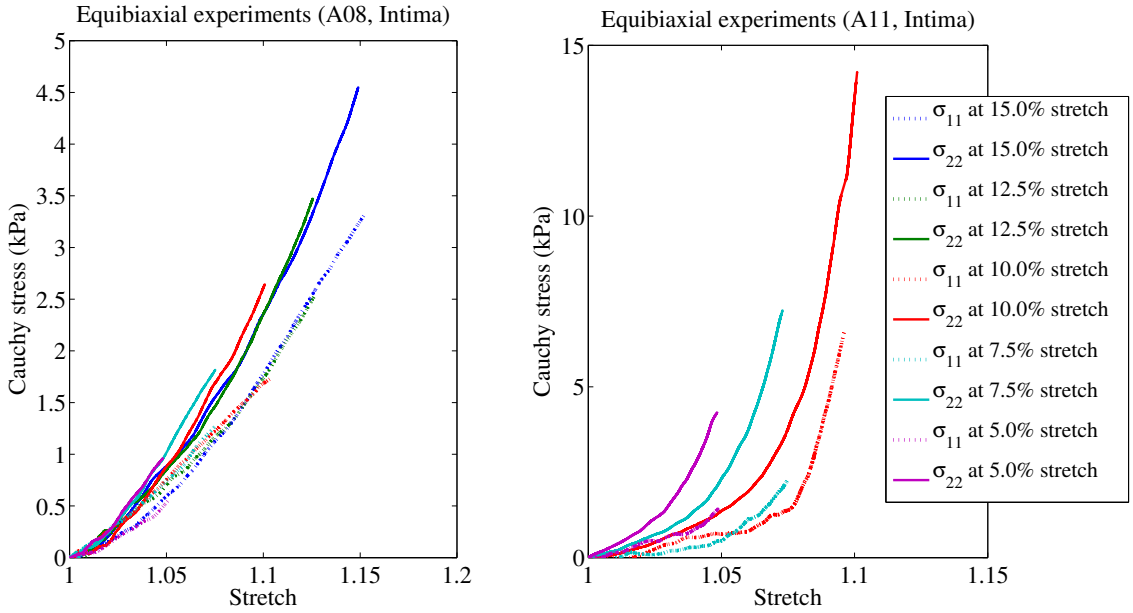

Figure 4.8: Stress vs. stretch diagrams of intimal layer of sample A08 and A11 showing the mechanical behavior of this layer in axial and cirumferential direction at different stretch levels.

4.5 Media

Tab. 4.11 and Tab. 4.12 show the maximum Cauchy stresses in axial and cirumferential direction of samples A01, A03 to A07 and A09 at different stretch levels (5% up to 15% in steps of 2.5%). Samples all show a square geometry and belong to the age group of donors above 60 years of age. A visualisation of Tab. 4.11 and Tab. 4.12 is presented in form of Whisker boxplots in Fig. 4.9. Stress vs. stretch diagrams of sample A01, A04 and sample A06 are shown in Fig. 4.10.

Table 4.11: Maximum Cauchy stresses in axial direction at different stretch levels for the medial layer. Median and IQR [Q1; Q3] at each stretch level are shown.

Stretch	1.050	1.075	1.100	1.125	1.150
$\lambda_1 = \lambda_2$	σ_{11} (kPa)	σ_{11} (kPa)	σ_{11} (kPa)	σ_{11} (kPa)	σ_{11} (kPa)
A01	0.85	1.67	2.32	3.22	4.69
A03	1.87	3.87	-	-	-
A04	0.38	0.82	1.23	1.68	2.28
A05	0.47	1.06	1.96	3.22	5.82
A06	0.44	0.81	1.48	1.79	2.54
A07	0.55	0.84	1.18	1.75	2.24
A09	0.76	1.05	1.37	-	-
$\tilde{x}$	0.55	1.05	1.42	1.79	2.54
IQR	[0.46; 0.81]	[0.83; 1.37]	[1.26; 1.84]	[1.79; 1.75]	[2.28; 4.69]

4.6 Adventitia

Tab. 4.13 and Tab. 4.14 show the maximum Cauchy stresses in axial and cirumferential direction of samples A01, A03 to A07 and A09 at different stretch levels (5% up to 15% in steps of 2.5%). Samples all show a square geometry and belong to the age group of donors above 60 years of age. A visualisation of Tab. 4.13 and Tab. 4.14 is presented in form of Whisker boxplots in Fig. 4.11. Stress vs. stretch diagrams of sample A06 and sample A09 are shown in Fig. 4.12. Fig. 4.13 shows non-linear stiffening of sample A02 at higher stretch levels (17.5% up to 27.5% stretch).

Table 4.12: Maximum Cauchy stresses in circumferential direction at different stretch levels for the medial layer. Median and IQR [Q1; Q3] at each stretch level are shown.

Stretch	1.050	1.075	1.100	1.125	1.150
$\lambda_1 = \lambda_2$	σ_{22} (kPa)	σ_{22} (kPa)	σ_{22} (kPa)	σ_{22} (kPa)	σ_{22} (kPa)
A01	1.35	2.20	3.10	4.01	5.35
A03	1.94	4.97	-	-	-
A04	0.30	0.89	1.29	1.83	2.55
A05	0.66	1.30	2.29	4.02	7.30
A06	0.91	1.71	2.60	3.38	4.43
A07	1.13	1.73	2.46	3.50	4.50
A09	1.29	1.72	2.21	-	-
$\tilde{x}$	1.13	1.72	2.38	3.50	4.50
IQR	[0.78; 1.32]	[1.50; 1.97]	[2.23; 2.57]	[3.38; 4.01]	[4.43; 5.35]

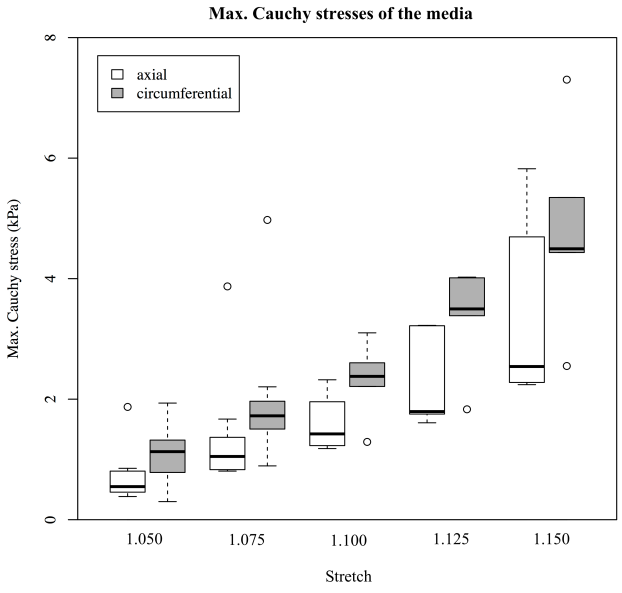

Figure 4.9: Whisker boxplot of the maximum cauchy stresses of the medial layer for sample A01, A03 to A07 and A09 at varying stretch levels. Values in axial direction are marked in white, while values in circumferential direction are marked in grey.

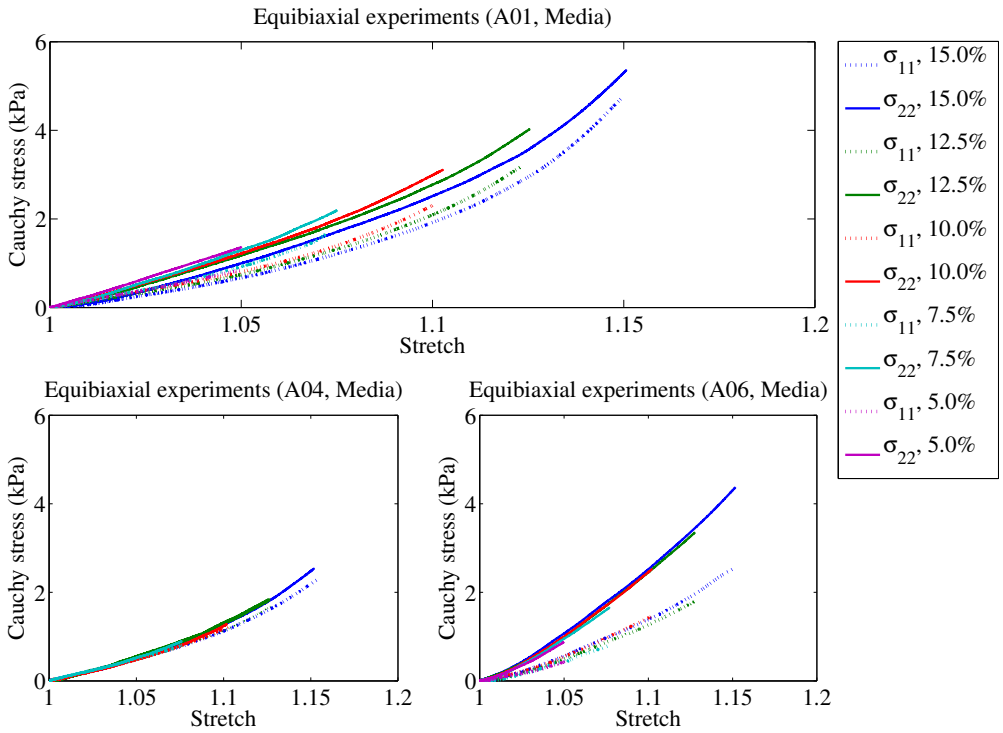

Figure 4.10: Stress vs. stretch diagram of medial layer of sample A01 (top), A04 (bottom left) and A06 (bottom right) showing the mechanical behavior of this layer in axial and cirumferential direction at different stretch levels.

Table 4.13: Maximum Cauchy stresses in axial direction at different stretch levels for the adventitial layer. Median and IQR [Q1; Q3] at each stretch level are shown.

Stretch	1.050	1.075	1.100	1.125	1.150
$\lambda_1 = \lambda_2$	σ_{11} (kPa)	σ_{11} (kPa)	σ_{11} (kPa)	σ_{11} (kPa)	σ_{11} (kPa)
A01	0.45	-	-	-	-
A03	0.10	-	0.31	-	-
A04	0.08	0.14	0.28	0.33	0.46
A05	0.13	0.08	0.19	0.23	0.51
A06	0.24	0.48	0.58	0.85	1.16
A07	0.07	0.09	0.13	0.18	0.22
A09	0.06	0.13	0.15	0.21	0.31
$\tilde{x}$	0.10	0.13	0.23	0.23	0.47
IQR	[0.07; 0.18]	[0.09; 0.14]	[0.16; 0.30]	[0.21; 0.33]	[0.31; 0.51]

Table 4.14: Maximum Cauchy stresses in circ. direction at different stretch levels for the adventitial layer. Median and IQR [Q1; Q3] at each stretch level are shown.

Stretch	1.050	1.075	1.100	1.125	1.150
$\lambda_1 = \lambda_2$	σ_{22} (kPa)	σ_{22} (kPa)	σ_{22} (kPa)	σ_{22} (kPa)	σ_{22} (kPa)
A01	0.86	-	-	-	-
A03	0.19	-	0.34	-	-
A04	0.07	0.15	0.41	0.53	0.65
A05	0.13	0.22	0.29	0.39	0.94
A06	0.30	0.54	0.77	1.06	1.44
A07	0.05	0.10	0.18	0.19	0.32
A09	0.12	0.23	0.29	0.41	0.59
$\tilde{x}$	0.13	0.22	0.32	0.41	0.65
IQR	[0.09; 0.24]	[0.15; 0.23]	[0.29; 0.40]	[0.39; 0.53]	[0.59; 0.94]

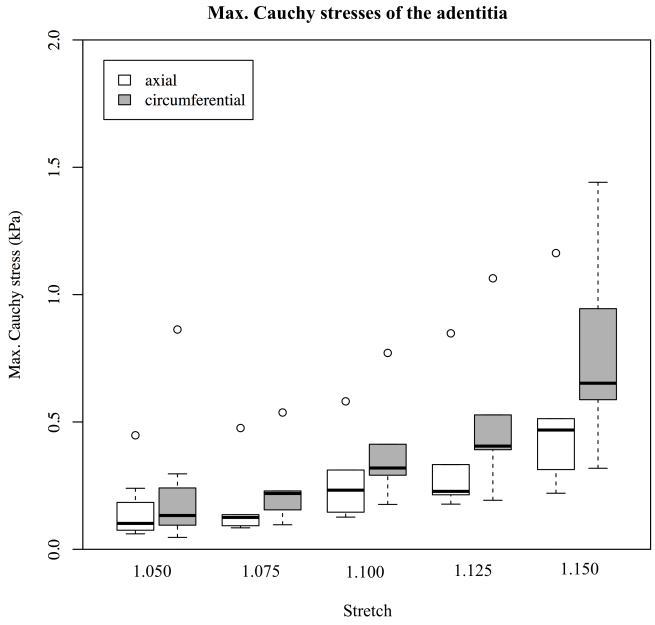

Figure 4.11: Whisker boxplot of the maximum cauchy stresses of the advenditial layer for sample A01, A03 to A07 and A09 at varying stretch levels. Values in axial direction are marked in white, while values in circumferential direction are marked in grey.

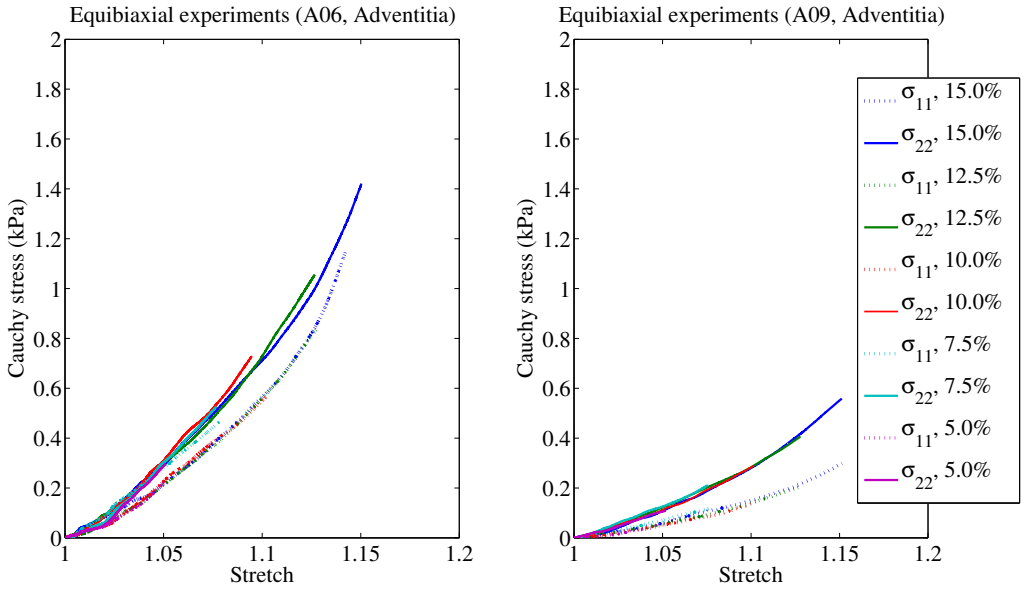

Figure 4.12: Stress vs. stretch diagrams of adventitial layer of sample A06 and A09 showing the mechanical behavior of this layer in axial and cirumferential direction at different stretch levels.

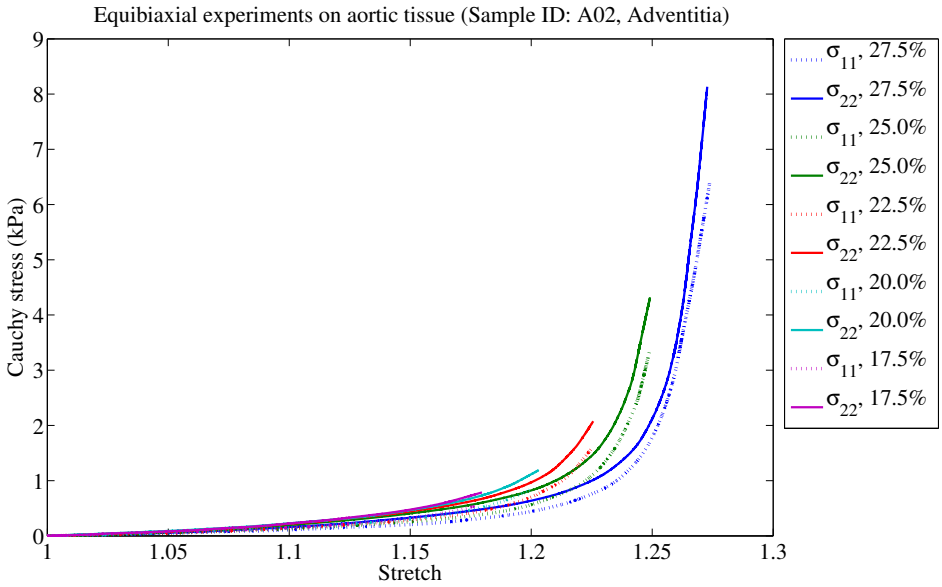

Figure 4.13: Stress vs. stretch diagram of adventitial layer of sample A02 showing the mechanical behavior of this layer in axial and cirumferential direction at higher stretch levels (17.5%, 20.0%, 22.5%, 25.0% and 27.5%).

4.7 Composite

Tab. 4.15 and Tab. 4.16 show the maximum Cauchy stresses in axial and cirumferential direction of samples A01, A03 to A07 and A09 at different stretch levels (5% up to 15% in steps of 2.5%). All samples show a square geometry and belong to the age group of donors above 60 years of age. A visualisation of Tab. 4.15 and Tab. 4.16 is presented in form of Whisker boxplots in Fig. 4.14. Stress vs. stretch diagrams of sample A06 and sample A09 are shown in Fig. 4.15.

Table 4.15: Maximum Cauchy stresses in axial direction at different stretch levels for the composite. Median and IQR [Q1; Q3] at each stretch level are shown.

Stretch	1.050	1.075	1.100	1.125	1.150
$\lambda_1 = \lambda_2$	σ_{11} (kPa)	σ_{11} (kPa)	σ_{11} (kPa)	σ_{11} (kPa)	σ_{11} (kPa)
A01	1.14	0.60	1.81	0.58	0.94
A03	0.53	0.96	1.33	1.82	2.46
A04	0.17	0.30	0.51	0.60	1.05
A05	0.58	-	-	-	-
A06	0.37	0.56	0.77	1.14	-
A07	0.24	0.34	0.41	0.53	0.62
A09	0.65	0.97	1.35	1.63	2.11
$\tilde{x}$	0.53	0.58	1.05	0.87	1.05
IQR	[0.31; 0.61]	[0.39; 0.87]	[0.58, 1.35]	[0.58; 1.51]	[0.94; 2.11]

4.8 Comparison of individual Layers and Composite

In order to compare the behavior of the individual layers and the composite the median and IQR of the max. Cauchy stresses resulting from equibiaxial tests were calculated at each stretch level. Tab. 4.17 shows the results in axial direction and Tab. 4.18 the results in circumferential direction. In order to visualize the distribution of data points n in terms of the median, the middle fifty percent (IQR), the smallest and biggest data point and potential outliers Whisker boxplots where generated as well as stripcharts. In Fig. 4.16 the distribution of the maximum Cauchy stresses for each individual layer and the composite in axial and circumferential direction at a stretch level of 15% is presented.

Table 4.16: Maximum Cauchy stresses in circumferential direction at different stretch levels for the composite. Median and IQR [Q1; Q3] at each stretch level are shown.

Stretch	1.050	1.075	1.100	1.125	1.150
$\lambda_1 = \lambda_2$	σ_{22} (kPa)	σ_{22} (kPa)	σ_{22} (kPa)	σ_{22} (kPa)	σ_{22} (kPa)
A01	1.15	1.30	3.14	1.12	1.81
A03	0.56	1.24	1.74	2.55	3.73
A04	0.17	0.25	0.54	0.69	1.47
A05	0.65	-	-	-	-
A06	0.47	0.65	0.84	1.39	-
A07	0.39	0.58	0.77	0.99	1.22
A09	0.62	0.90	1.38	1.76	2.37
$\tilde{x}$	0.56	0.77	1.11	1.26	1.81
IQR	[0.43; 0.63]	[0.59; 1.15]	[0.78; 1.65]	[1.02; 1.67]	[1.47; 2.37]

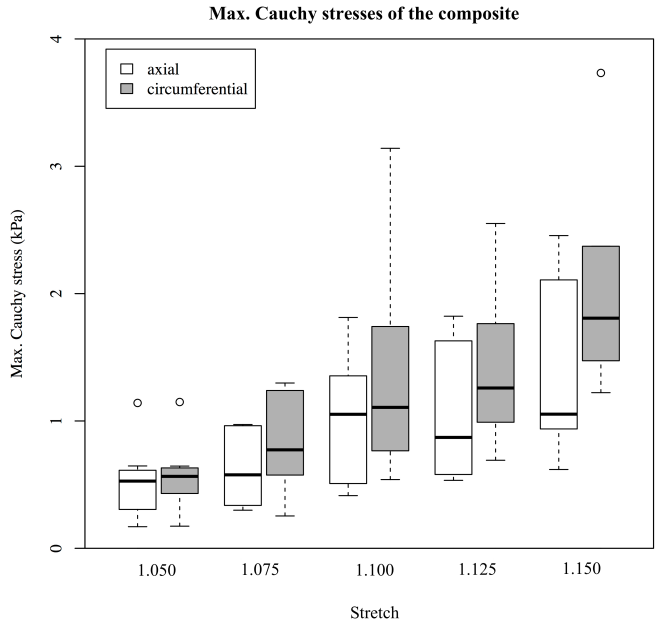

Figure 4.14: Whisker boxplot of the maximum cauchy stresses of the composite for sample A01, A03 to A07 and A09 at varying stretch levels. Values in axial direction are marked in white, while values in circumferential direction are marked in grey.

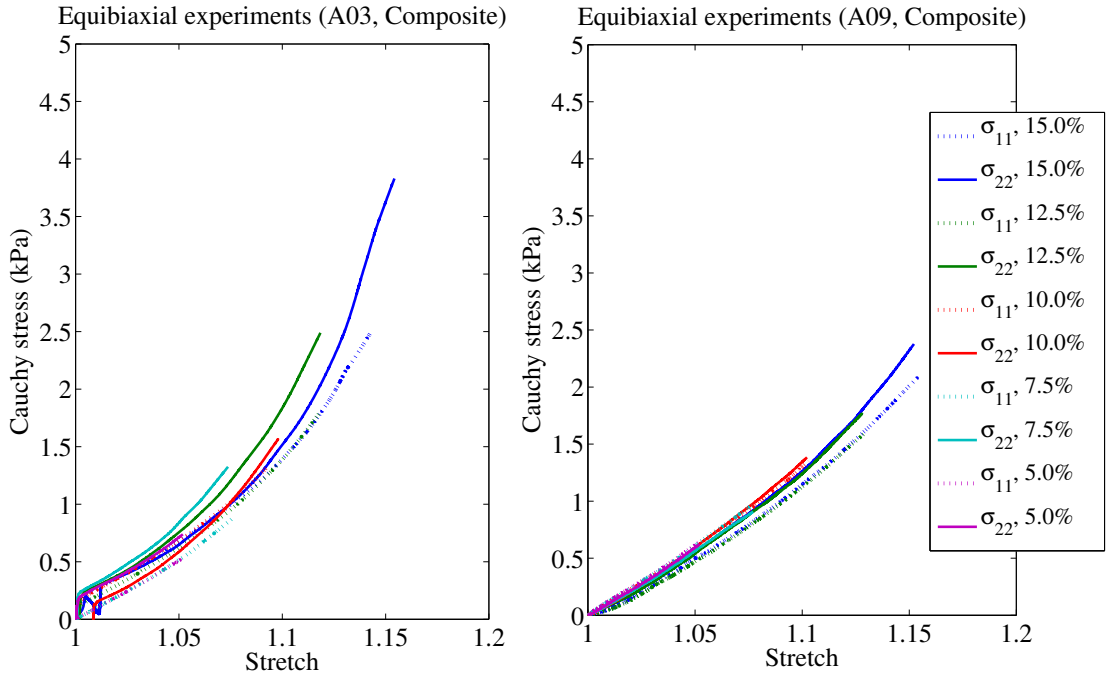

Figure 4.15: Stress vs. stretch diagrams of composite of sample A03 and sample A09 showing the mechanical behavior of the tissue in axial and cirumferential direction at different stretch levels.

Table 4.17: Summary of median and IQR of max. Cauchy stresses in axial direction (σ_{11}) for each individual layer and the composite at different stretch levels (Sample A01 to A11). The number of data points n used for the calculations of the median an IQR varied between layers and stretch levels.

Stretch	Intima			Media			Adventitia			Composite		
$\lambda_1 = \lambda_2$	n	$\tilde{x}$ (kPa)	IQR (kPa)	n	$\tilde{x}$ (kPa)	IQR (kPa)	n	$\tilde{x}$ (kPa)	IQR (kPa)	n	$\tilde{x}$ (kPa)	IQR (kPa)
1.050	3	1.47	[1.07; 4.02]	11	0.59	[0.46; 0.90]	11	0.13	[0.08; 0.25]	11	0.58	[0.40; 1.07]
1.075	2	1.85	[1.63; 2.06]	11	1.06	[0.83; 1.31]	9	0.14	[0.12; 0.32]	10	0.83	[0.57; 1.61]
1.100	2	4.23	[3.01; 5.46]	10	1.55	[1.26; 2.03]	10	0.29	[0.16; 0.49]	9	1.33	[0.77; 1.81]
1.125	1	2.72	[2.72; 2.72]	8	1.98	[1.73; 3.22]	8	0.28	[0.22; 0.69]	8	1.24	[0.59; 1.68]
1.15	1	3.36	[3.36; 3.36]	9	2.54	[2.28; 4.69]	8	0.49	[0.33; 0.93]	7	1.72	[1.00; 2.28]

Table 4.18: Summary of median and IQR of max. Cauchy stresses in circumferential direction (σ_{22}) for each individual layer and the composite at different stretch levels (Sample A01 to A11). The number of data points n used for the calculations of the median an IQR varied between layers and stretch levels.

Stretch	Intima			Media			Adventitia			Composite		
$\lambda_1 = \lambda_2$	n	$\tilde{x}$ (kPa)	IQR (kPa)	n	$\tilde{x}$ (kPa)	IQR (kPa)	n	$\tilde{x}$ (kPa)	IQR (kPa)	n	$\tilde{x}$ (kPa)	IQR (kPa)
1.050	3	4.28	[2.78; 11.98]	11	1.19	[0.78; 1.32]	11	0.19	[0.12; 0.34]	11	0.63	[0.52; 1.09]
1.075	2	4.63	[3.29; 5.96]	11	1.73	[1.50; 2.12]	9	0.23	[0.18; 0.54]	10	1.12	[0.71; 1.69]
1.100	2	8.42	[5.55; 11.28]	10	2.53	[2.23; 3.06]	10	0.38	[0.29; 0.71]	9	1.41	[0.84; 3.14]
1.125	1	3.57	[3.57; 3.57]	8	3.62	[3.03; 4.02]	8	0.47	[0.39; 1.03]	8	1.58	[1.09; 2.04]
1.150	1	4.67	[4.67; 4.67]	9	4.50	[4.06; 5.79]	8	0.80	[0.58; 1.32]	7	2.37	[1.64; 3.05]

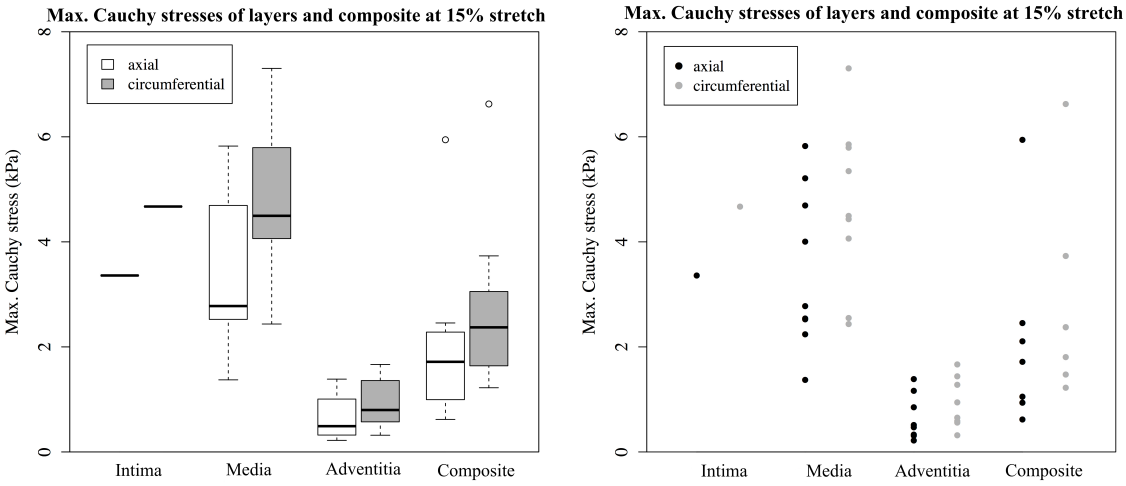

Figure 4.16: Whisker boxplot of the maximal cauchy stresses of the individual layers and the composite of all samples at a stretch level of 15% (left). Max. Cauchy stresses in axial direction are shown in white, whereas max. Cauchy stresses in circumferential direction are shown in grey. On the right hand side the corresponding stripcharts are shown, displaying the individual data points in axial direction in black and data points in circumferential direction in grey.

5 Discussion

The results in relation to age, gender and geometry for the individual layers are discussed in the following chapter. Conclusions are made, open problems are shown and the future outlook on this study is presented.

5.1 Age-related Mechanical Behavior

The mechanical behavior of the abdominal aorta shows major differences in relation with age. Accoording to [34] samples can be divided into three groups based on the age of the donor. Samples of donors younger than 30 years fall within the first group, older than 30 years and up to 60 years into the second group and donors aged above 60 years in the third group. Hence, the samples of this study could be divided into two age groups with samples A02, A08 and A10 belonging to the group of donors 60 years of age and younger and samples A01, A03 to A07, A09 and A11 to the group aged above 60 years of age. The maximum Cauchy stresses of the samples of the two groups were compared at different stretch levels in axial and circumferential direction for the media, the adventitia and the composite. The intima was not taken in account as there was not enough data of this layer available in order conclude sufficiently. Only the media showed increased maximum Cauchy stresses in relation to advancing age, while the behavior of the adventitia and the composite seemed to exhibit opposite reaction (see Fig. 4.1 and Fig. 4.2). An explanation for this unexpected result could be gender related influences (see section 5.2 for further investigations) or/and influences of the specimen geometry of the samples (see section 5.3) on the mechanical behavior of the tissue falsifying the outcome of the above mentioned comparison. To cross out the gender and geometry related influences the Cauchy stress vs. stretch diagram of the composite was compared (see Fig. 4.3) for sample A02 (donor 45 years of age) and sample A03 (donor 82 years of age) both originating from a male donor and sharing the same specimen geometry (20x20 mm). Sample A03 shows slightly higher maximum Cauchy stresses for stretch levels up to 12.5%, while stiffening occurs at a stretch of 15%. The mechanical behavior of sample A02 is very linear for all stretch levels. The medial layer of sample A03 ruptured at the attachment points of the hooks at a stretch level of 10% showing indications of stiffening in preceding stretch levels. Similar to the medial layer the adventitia ruptured at a stretch level of 12.5% for sample A03. For

sample A02 both layers showed linear elastic behavior for all stretch levels. This suggest that within the tested samples an age related change in mechanical behavoir in terms of stiffening can be observed for all layers when effects of gender and varying specimen geometry are limited.

5.2 Gender-dependent Mechanical Behavior

Samples of male donors (A01, A03, A04 and A07) were compared with samples of female donors (A05, A06 and A09) to show a potential influence of the gender on the mechanical response of the individual tissue layers as well as the composite. For the comparison only samples of the same geometry (20x20 mm) and within the same age group (above 60 years of age) were used to secure elimination of age or geometry related changes in the mechanical response. As there was only an insufficient amount of data available for the intimal layer additionally following a cruciform geometry this layer was not considered in this comparison. Looking at Tab. 4.4, Tab. 4.5, Tab. 4.6, Fig. 4.4 and Fig. 4.5 no clear relation between the mechanical behavior and the genders of the donors of specific samples is visible. The medial layer, for instance, shows a stiffer behavior for samples originating from male donors at 5% stretch in axial as well as circumferential direction. At a stretch level of 10% in axial direction the media exhibits a contrariwise mechanical behavior, while agreeing with results at 5% stretch in circumferential direction. Comparisons for the adventitia and the composite showed similar arbitrary outcomes.

5.3 Geometry-dependend Mechanical Behavior

The influence of the sample geometry on the mechanical behavior of the media, the adventitia and the composite was investigated by comparing the maximum Cauchy stresses of a sample with square shaped geometry (A09) with one of cruciform geometry (A10). As the intima was only tested in a cruciform shape, making a more sensitive preparation and mounting procedure without harming the tissue possible, this layer was not part of the comparison. Higher maximum Cauchy stresses could be observed for sample A10 for the medial and advenditial layer as well as the composite in both directions (see Tab. 4.7, Tab. 4.8, Tab. 4.9). Sample A11 (cruciform shape) shows similiar results to sample A10 (see Fig. 4.6 for a comparison with sample A09). This could be explained through an uneven distribution of load and therefore an inhomogenous strain field within the central region (5x5 mm) of the cruciform specimen (see Fig. 4.7). The cause of this uneven distribution could be the increased thickness of the media, adventitia and composite in comparison to the intima. Age-related influences falsifying this analysis can be obviated due to an age difference of only five/two years between donors of sample A09 and A10/A11.

5.4 Intima

To enable biaxial tensile testing of this fragile layer the cruciform specimen geometry was introduced. The ideal preparation procedure is currently assessed. The intima could only be tested for three of the 11 samples. Maximum Cauchy stresses vary strongly within the tested specimens (see Tab. 4.10). Sample A10 showed stiffening at 5% stretch rupturing at a stretch level of 7.5%. Similar to sample A11, which showed failure at 12.5% stretch (see Fig. 4.8). Sample A08 showed linear elastic behavior up to a stretch level of 15% (see Fig. 4.8). This difference in mechanical behavior may be related to age as the donor of sample A08 was significantly younger than donors of the other two samples. Differing thicknesses of the samples as well as a slight variation in the specimen preparation and the mounting process could also contribute to the observed differences in the mechanical behavior of samples A08, A10 und A11. All sample show higher Cauchy stresses in cirumferential direction. The distinct stiffer reponse in circumferential direction can be explained through the intima's underlying structure.

5.5 Media

Considering the age and geometry related change in mechanical behavior of this layer only samples belonging to the same age group (above sixty years of age) and same shape (20x20 mm) were used for comparison (A01, A03 to A07 and A09). A05 to A07 exhibit very similar behavior up to a stretch level of 12.5% (see Fig. 4.9). At 15% stretch sample A05 shows non-linear stiffening, while sample A06 and A07 still show linear elastic behavior. Sample A04 shows smaller maximum Cauchy stresses in both directions, whereas Sample A01 and A03 exhibit higher maximum Cauchy stresses compared to the rest of the samples (see Fig. 4.10). This might be due to the more advanced age of the donors (84 and 82) of these samples. Sample A09 behaves similar to sample A01. The mechanical behavior of the media is highly anisotropic and behaves linear elastic in the lower stress regions. Non-linear stiffening of this layer starts at a stretch levels of 15% and higher.

5.6 Adventitia

For the comparison of the mechanical response of the individual specimen of this layer the same samples were chosen as for the media (A01, A03 to A07 and A09). Examining Tab. 4.13 and Tab. 4.14 one can see that sample A07 and A09 behave very similiar in axial direction with sample A09 showing a slightly stiffer behavior in circumferential direction (see Fig. 4.12) similar to sample A04. Nevertheless, the mechanical response of sample

A07, A09 and A04 is linear elastic not showing any signs of non-linear stiffening. Sample A01 ruptured at a stretch level of 7.5% and its values of the maximum Cauchy stresses in both directions at 5% stretch are shown as outliers in Fig. 4.11. A03 failed at 12.5% stretch. These two samples belong to the donors of the most advanced age (84 years and 82 years of age) possibly explaining the early rupture. The outliers at all other stretch levels (see Fig. 4.11) correspond to sample A06 showing higher Cauchy stresses at mentioned stretch levels compared to other samples (also see Fig. 4.12) showing slight stiffening at a stretch level of 15%. The overall mechanical behavior of the adventitia is slightly anisotropic behaving linear elastic in the lower stress regions. Non-linear stiffening of this layer starts at a stretch levels of 20% and higher (see Fig. 4.13). As non of the samples used for comparison were tested up to stretch levels were stiffening kicks in this effect was shown for sample A02 belonging to the age group 60 years and younger.

5.7 Composite

Same samples were chosen for the comparison of the composite as for the media and adventitia. Tab. 4.15 and Tab. 4.16 show that sample A01 seems to exhibit stiffening at a stretch level of 10% followed by lower values of maximum Cauchy stresses at 12.5% and 15%. This behavior may be explained through improper prestretching. The high age of the donor (84 years) of this sample could have also played an influencing role. The outliers at 5% stretch in axial and circumferntial direction presented in Fig. 4.14 originated from the values of the maximum Cauchy stresses of this sample. Sample A03 behaves similar to sample A09 (see Fig. 4.15) with sample A03 showing stiffening at 15% stretch (shown as outelier in cirumferential direction in Fig. 4.14). The lowest maximum cauchy stresses belong to sample A04. Sample A05 showed rupture at 7.5% stretch and sample A06 at 12.5% stretch. The differences in the mechanical response of the samples may be explained through the varying thickness of the samples, inconstant sample preparation or variations in the mounting procedure.

5.8 Comparison of individual Layers and Composite

Maximum Cauchy stresses could only be compared at stretch levels up to 15%. This is due to the lacking data in the higher stretch ranges. As the Intima could only be tested for samples A08, A10 and A11 the results for this layer are only partly significant. Anyhow, this layer seems to exhibit the stiffest behavior with a pronounced anisotropy (see Fig. 4.16). According to [7] the intima does not contribute in a major way to the solid mechanical properties of the arterial wall. Nevertheless, this layer tends to thicken and stiffen with age making its mechanical contribution more important [7].

The medial layer shows the second highest maximum Cauchy stresses in axial as well as circumferential direction (see Fig. 4.16). Similar to the intima the mechanical response of the media is highly anisotropic showing an significant stiffer behavior in circumferential direction relating to the internal structure of the media [12]. A strong difference within the response of the different samples (A01 to A11) can be observed. As suggested above this might be due to the alternating geometry and thickness of the samples as well as the varyingn age of the donors.

The smallest maximum Cauchy stresses are exhibited by the adventitia (see Fig. 4.16), which corresponds well with the properties described in literature where this layer is said to be linear elastic until a certain pressure is reached. At higher pressures the wavy collagen fibres of this structure are fully straightened leading to an significant increase of stiffness [7]. As only data of stretch levels up to 15% for all layers could be compared the stiffening of this layer is not visible in Fig. 4.16. Anyhow, the effect of the fully straightened collagen fibres on the overall response of the adventitial layer can be observed in Fig. 4.13. The anisotropic behavior of this layer is not as pronouced as in the intimal and medial layer for low stretch levels as collagen fibres do not contribute to the mechanical response. Only the extracellular matrix, which is said to be isotropic, contributes to the mechanical behavior. Strong anisotropy is usually based on the contribution of collagen to the mechnical response.

The composite structure shows a stiffer character than the adventitia not reaching the stiffness of the media (see Fig. 4.16) as properties of both of those layers contribute to the overall mechanical response of the composite. The outliers shown for this layer belong to sample A10 (cruciform specimen), which underlines the assumption that the cruciform specimen geometry is not suitable for testing the composite structure. The maximum Cauchy stresses of the composite tested in this geometry are significantly higher as a homogenous distribution of loads is not possible due to the increased thickness of the composite compared to the adventitia and intima.

All layers, except the intima, behaved linear elastic up to a stretch level of 12.5%. The adventitia and the composite showed stiffening effects starting at a stretch level of 20.0% and the media at a stretch level of 15% for some samples. Stiffening of the intima seemed to start at a stretch level of 5%.

5.9 Conclusion

The distinct influence of age on the mechanical behavior of the tissue, in terms of stiffening, could only be shown for the media. Nevertheless, it is known that the elastin content decreases with age as the collagen content increases potentially explaining this stiffening effect with age [16]. A change in mechanical behavior due to gender differences of the

donors could not be observed. In contrary, the geometry of the samples showed an major impact on the mechanical behavior. The mechanical response of the media, the adventitia and the composite exhibited much higher maximum Cauchy stresses when tested as a cruciform specimen compared to the square shape. This may be due to an uneven distribution of loads in the central region (5x5 mm) of this certain shape caused by the increased thickness compared to the intimal layer. All layers showed an anisotropic but linear elastic behavior in lower stress regions followed by non-linear stiffening at higher stretch levels. The intima showed stiffening effects at stretch levels as low as 5%, while the media and composite showed a similar effect at stretch levels of 15% and above. The advenditia stiffened at stretch levels of 20% and above. The intima and the media showed a more distinct anisotropy than the adventitia and the composite. The intima exhibited the highest Cauchy stresses for the stretch levels tested (5% up to 15% in steps of 2.5%) followed by the media, the composite and the adventitia.

5.10 Open Problems

Often occuring problems in experimental biomechanics include the accessibility and number of samples of similar age, thickness and history of health in order to be able to make a valid comparison. Different conservation times of the samples may potentially influence the results and should therefore be standardised. Further, the preparation procedure and mounting process of the samples is also subjected to variations.

5.11 Future Outlook

As part of a research project of the Institute of Biomechancis, Technical University Graz, Austria, in cooperation with the Institute of Pathology, University Clinic Graz, Austria, this master thesis provides biaxial experimental data of the individual layers of healthy abdominal aortas. The results of this study will be further used for comparison with diseased tissue, namely AAAs, and for formulating constitutive laws as well as finite element analysis. Structural analysis of the samples was done, which gives more insight on the tissue's microscopic level also making more precise thickness measurements possible.

Bibliography

[1] G. A. Holzapfel and M. Unterberger. Introduction to biomechanics. University Lecture, 2012. Insitute of Biomechanics, University of Technology Graz, Austria.

[2] J. D. Humphrey and G. A. Holzapfel. Mechanics, mechanobiology, and modeling of human abdominal aorta and aneurysms. *Journal of Biomechanics*, pages 805–814, 2012.

[3] Johns Hopkins University. Johns hopkins medicine - heart and vascular institute, 03 2015. URL `http://www.hopkinsmedicine.org/heart_vascular_institute/conditions_treatments/conditions/aorta.html`.

[4] Circulation Foundation. Circulation foundation - help and advice, March 2015. URL `http://www.circulationfoundation.org.uk/help-advice/`.

[5] G. M. Novaro. Diseases of the aorta, 04 2014. URL `http://www.clevelandclinicmeded.com/medicalpubs/diseasemanagement/cardiology/diseases-of-the-aorta/`.

[6] T. E. Carew, R. Vaishnav, and D. J. Patel. Compressibility of the arterial wall. *Circulation Research*, pages 61–68, 1968.

[7] G. A. Holzapfel, T. C. Gasser, and R. W. Ogden. A new constitutive framework for arterial wall mechanics and a comparative study of material models. *Journal of elasticity and the physical science of solids*, pages 1–48, 2000.

[8] R. W. Ogden. *Biomechanical Modelling at the Molecular, Cellular and Tissue Levels*, chapter Anisotropy and Nonlinear Elasticity in Arterial Wall Mechanics, pages 179 – 258. Springer Wien NewYork, 2009. CISM Courses and Lectures, vol. 508.

[9] R. P. Vito and H. Demiray. A two layered model for arterial wall mechanics. In *Proc. 35th Ann. Conf. Engineering in Medicine and Biology (ACEMB), Pennsylvania*, 1982.

[10] G. Sommer. *Mechanical properties of healthy and diseased human arteries: insights into human arterial biomechanics and related material modeling*. Verlag der Techn. Univ. Graz, 2010.

[11] P. D. Richardson. Biomechanics of plaque rupture: progress, problems, and new frontiers. *Annals of biomedical engineering*, pages 524–536, 2002.

[12] M. H. Ross and W. Pawlina. *Histology - A text and atlas*. Lippincott Williams & Wilkins, 2011.

[13] Rice University. Anatomy & physiology, March 2013. URL `http://cnx.org/contents/14fb4ad7-39a1-4eee-ab6e-3ef2482e3e22@6.5:132/Anatomy_&_Physiology`. CNX Anatomy and Physiology.

[14] J. D. Humphrey. *Biomechanical Modelling at the Molecular, Celllular and Tissue Levels*, chapter Need for Continuum Biochemomechanical Theory of Soft Tissue and Cellular Growth and Remodeling, pages 1–82. Springer Wien NewYork, 2009. CISM Courses and Lectures, vol. 508.

[15] B. H. Strauss and M. Rabinovitch. Adventitial fibroblasts: defining a role in vessel wall remodeling. *American journal of respiratory cell and molecular biology*, pages 1–3, 2000.

[16] G. A. Holzapfel. Mechancis of biological tissues. University Lecture, 2014. Institute of Biomechanics, University of Technology Graz, Austria.

[17] B. Alberts, D. Bray, K. Hopkin, A. Johnson, J. Lewis, M. Raff, K. Roberts, and P. Walter. *Essential cell biology*. Garland Science, 2013.

[18] M. R. Roach and A. C. Burton. The reason for the shape of the distensibility curves of arteries. *Canadian journal of biochemistry and physiology*, pages 681–690, 1957.

[19] MedicineNet. Definition of abdominal aorta, 2015. URL `http://www.medicinenet.com/script/main/art.asp?articlekey=8631`.

[20] Anatomyee. Branches of the abdominal aorta, 2015. URL `http://www.anatomyee.com/branches-abdominal-aorta/`.

[21] J. D. Humphrey. *Cardiovascular solid mechanics: cells, tissues, and organs*. Springer Science & Business Media, 2002.

[22] A. Eilaghi, J. G. Flanagan, G. W. Brodland, and C. R. Ethier. Strain uniformity in biaxial specimens is highly sensitive to attachment details. *Journal of biomechanical engineering*, page 0910031 0910037, 2009.

[23] S. Sherifova. Modeling the propagation of aortic dissection. Master's thesis, KTH Stockholm, Sweden and Technical University Graz, Austria, 2015.

[24] J. D. Humphrey, D. L. Vawter, and R. P. Vito. Quantification of strains in biaxially tested soft tissues. *Journal of Biomechanics*, pages 59–65, 1987.

[25] D. C. Haspinger. Quantification of shear stresses and strains in biaxially tested human myocardium. Bachelor thesis, University of Technology Graz, Austria, 2013.

[26] Messphysik. Spezialprüfmaschinen, 2016. URL `http://www.messphysik.com/fileadmin/messphysikdaten/Download/01_957_Biaxialpruefmaschine_PI_DE.pdf`. Accessed: 2016-01-14.

[27] R. Kresnik. Biaxial mechanical investigation of human ventricles myocardium. Diploma thesis, University of Technology Graz, Austria, 2012.

[28] K. Hayashi. Experimental approaches on measuring the mechanical properties and constitutive laws of arterial walls. *Journal of biomechanical engineering*, pages 481–488, 1993.

[29] G. Thallinger. Statistics and experimental design. University Lecture, 2012. Insitute of molecular Biotechnology, University of Technology Graz, Austria.

[30] M. Zemánek, J. Bursa, and M. Deták. Biaxial tension tests with soft tissues of arterial wall. *Engineering Mechanics*, pages 3–11, 2009.

[31] Y. C. Fung. Biomechanics: material properties of living tissues, 1993.

[32] B. D. Stemper, N. Yoganandan, M. R. Stineman, T. A. Gennarelli, J. L. Baisden, and F. A. Pintar. Mechanics of fresh, refrigerated, and frozen arterial tissue. *Journal of Surgical Research*, pages 236–242, 2007.

[33] R. T. Venkatasubramanian, E. D. Grassl, V. H. Barocas, D. Lafontaine, and J. C. Bischof. Effects of freezing and cryopreservation on the mechanical properties of arteries. *Annals of Biomedical engineering*, pages 823–832, 2006.

[34] J. P. Vande Geest, M. S. Sacks, and D. A. V. Age dependency of the biaxial biomechanical behavior of human abdominal aorta. *Journal of biomechanical engineering*, pages 815–822, 2004.